Ocean carbon transport in a box-diffusion versus a general circulation model

Fortunat Joos

Physics Institute, University of Bern, Bern, Switzerland

James C. Orr

Laboratoire de Modélisation du Climat et de l'Environnement, CEA/DSM, Gif-sur-Yvette, France

Ulrich Siegenthaler [1]

Physics Institute, University of Bern, Bern, Switzerland

Abstract. We have compared vertical transport of temperature, anthropogenic CO_2, natural radiocarbon (^{14}C), and bomb ^{14}C in a global box-diffusion model (B-D) and a three-dimensional (3-D) ocean general circulation model from the Geophysical Fluid Dynamics Laboratory. Our main objectives were (1) to test the eddy diffusion parameterization of large-scale vertical transport in ocean box models and (2) to assess the utility of bomb-produced and natural ^{14}C observations to validate ocean models used to estimate anthropogenic CO_2 uptake. From the 3-D model's distributions and fluxes of natural ^{14}C, bomb ^{14}C, and anthropogenic CO_2, we have calculated apparent diffusivities (K_{ap}) vertically over the global ocean that range mostly between 4000 and 8000 m^2 yr^{-1}. These K_{ap} agree quantitatively with diffusivities found by fitting B-D models to observed distributions of natural and bomb ^{14}C. We then used these sets of K_{ap} in different runs of a global B-D model. Results from all B-D models runs matched to within 13% those from the 3-D model for global uptake of anthropogenic CO_2 and bomb-^{14}C penetration depth. Although K_{ap} from 3-D simulations for bomb ^{14}C vary with time, those from 3-D runs for anthropogenic CO_2 are essentially constant. Still, we found nearly the same results with the B-D model when K_{ap} from 3-D bomb ^{14}C simulations are approximated as time invariant. The best agreement (within 3%) between 3-D CO_2 simulations and B-D model runs was found when applying K_{ap} derived from bomb ^{14}C in the surface and from natural ^{14}C in the deep. Agreement was worse when using K_{ap} from 3-D simulations for anthropogenic CO_2 itself, mostly because in this case deeper K_{ap} could only be extrapolated from higher surface values. We have found it appropriate to study global oceanic uptake of anthropogenic CO_2 with B-D model and to validate anthropogenic carbon uptake models using natural and bomb ^{14}C observations. For bomb ^{14}C in the 3-D model, convective transport was most important during 1955-1964 while atmospheric levels were rising; afterward, atmospheric levels drop, and advective overturning dominates as for natural ^{14}C. Thus ^{14}C seems less than ideal to validate the convective scheme of general circulation models.

1. Introduction

Parameterized box models are widely used to describe the transport of tracers in the ocean-atmosphere sys-

tem as a means to study both the global climate [e.g., *Siegenthaler and Oeschger*, 1984; *Harvey*, 1986; and *Schlesinger and Jiang*, 1990] and the global carbon cycle [e.g., *Oeschger et al.*, 1975; *Siegenthaler and Wenk*, 1984; *Broecker and Peng*, 1987; *Siegenthaler and Joos*, 1992; *Hesshaimer et al.*, 1994]. Although general circulation models (GCMs) are more realistic, simple box models do have some distinct advantages: (1) they demand much less computing resources thereby allowing many sensitivity studies; (2) they are relatively easy to calibrate (i.e., to tune to match observations); and (3)

---

[1]Deceased July 14, 1994.

model output is easier to interpret than that of GCM's. However, all transport processes in box models are parameterized, in contrast to GCMs which are based on the physical laws of motion. This study has attempted to determine to what extent the widely used eddy diffusivity parameterization is justified in box-modeling studies.

For global carbon-cycle studies, natural and bomb-produced ^{14}C are of interest because ocean models used to estimate uptake of anthropogenic CO_2 are typically calibrated (or validated, in the case of two-dimensional (2-D) and three-dimensional (3-D) models) by comparing their simulated ^{14}C distribution versus those measured in the real ocean [e.g., *Revelle and Suess*, 1957; *Oeschger et al.*, 1975; *Maier-Reimer and Hasselmann*, 1987; *Toggweiler et al.*, 1989a, b; *Siegenthaler and Joos*, 1992; *Enting et al.*, 1994]. Unfortunately, it has never been tested if model calibration using radiocarbon observations is appropriate.

The main purposes of this paper are (1) to evaluate the eddy diffusivity parameterization as used in simple box models and (2) to study how well the penetration of bomb-produced radiocarbon into the ocean serves as an analog for oceanic uptake of anthropogenic CO_2. We found that the diffusion approach is justified to study the oceanic uptake of transient tracers if transport is parameterized for large spatial scales (basin; global ocean) and typical timescales exceed 10 years. We also found that bomb-^{14}C observations are well suited to tune box-diffusion type models designed to calculate the oceanic uptake of anthropogenic CO_2. On the other hand, temperature was found to be unsuitable to determine transport coefficients for parameterized carbon cycle models.

Frequently, tracer transport in box models is described by a linear flux-gradient relationship, expressed as Fickian diffusion (often called eddy diffusion because it concerns large, nonmolecular scales, where eddies transport mass between two regions); sometimes this relationship is combined with advective terms. In its one-dimensional (1-D) form, such transport across a horizontal plane can be represented as

$$f = -k\frac{\partial C}{\partial z} + wC \qquad (1)$$

where f is the mean tracer flux per unit area, k is the eddy diffusivity, $\partial C/\partial z$ is the spatially averaged gradient, C is the mean tracer concentration, and w is the average water velocity for the area under consideration. Thus one assumes that the flux through a large area is a function of spatially averaged quantities. Usually, it is also assumed that the eddy diffusivity k is independent of the tracer's distribution, sources, and sinks and that k does not vary with time. Yet these assumptions remain largely untested, despite widespread use of the eddy diffusion approach in box models of the ocean [e.g., *Enting et al.*, 1994].

There have been a few studies, however, that have addressed the eddy-diffusion parameterization. One study

by *Mahlman* [1975] compared atmospheric tracer transport in 1- and 2-D eddy-diffusion models to that in a GCM. Mahlman calculated so-called apparent eddy diffusivities, K_{ap}, from the output of an atmospheric GCM by solving equation (1) for the diffusivity coefficient. He first calculated spatially averaged fluxes and gradients; then he divided the averaged fluxes by the appropriate averaged gradients, thereby neglecting the advection term in equation(1). In this way, apparent diffusivity coefficients were determined for spatially aggregated regions for each of several simulated tracers. Mahlman found that even the best set of parameters derived to fit the observed values of one particular tracer may not be applied to a tracer with a different distribution, sources, and sinks. As an aside, *Plumb and Mahlman* [1987] offer a nice example of the utility of K_{ap} derived from a 3-D atmospheric model, i.e., to drive a 2-D zonal mean model having the same vertical and latitudinal resolution. The latter model has received widespread use in the atmospheric modeling community [e.g., *Ciais et al.*, 1995].

As for the ocean, *Sarmiento* [1983] calculated K_{ap} for tritium in the North Atlantic at different times from vertical fluxes simulated in a regional version of the 3-D ocean model from the Geophysical Fluid Dynamics Laboratory (GFDL). He found K_{ap} for tritium to vary with time.

Expanding upon the above two approaches, *Siegenthaler and Joos* [1992] considered the mean advective terms for their simple box model. They derived the advective component of K_{ap} from the tracer fluxes due to vertical advection, as simulated by a global version of the GFDL 3-D model [*Toggweiler et al.*, 1989a]. Siegenthaler and Joos's two sets of K_{ap} from the 3-D simulations for temperature and natural ^{14}C differ substantially because these two tracers have different spatial distributions. Furthermore, temperature variations on isopycnal surfaces are small; therefore heat transport to depth by isopycnal mixing does not play an important role. Siegenthaler and Joos also found good agreement between their K_{ap} derived from the GCM's natural ^{14}C fluxes versus those obtained by fitting their high-latitude exchange/interior diffusion-advection (HILDA) model to observed distributions of ^{14}C.

Unfortunately, the number of observations is insufficient to pursue our two main objectives, that is, testing the eddy diffusion transport approach in box models of the ocean and testing the utility of bomb ^{14}C as an analog for anthropogenic CO_2. Instead, we used, as have previous studies, a 3-D general circulation model as the best available substitute for real ocean processes. This paper goes beyond the work of *Siegenthaler and Joos* [1992] by considering two additional tracers, bomb-produced ^{14}C and anthropogenic CO_2, and by distinguishing not only the advective portion of the total K_{ap} from the 3-D model, but also other components due to convection and explicit diffusion.

Concerning the validation of carbon-cycle models, it follows from the tracer-independent fields of advection

and convection that transport of different passive tracers to depth is identical when the spatial and temporal distributions of the tracers are the same. To compare tracer distributions, we have first analyzed the latitudinal variations of the zonally averaged surface tracer concentration in dimensionless units. Concentrations have been scaled using the average surface concentration and the mean surface-to-deep sea gradient. Our comparison of these normalized distributions revealed that the fields of ^{14}C and CO_2 are similar, whereas the temperature field is much different. Next, we have compared K_{ap} derived from the GCM's distribution of natural and bomb-produced ^{14}C with those from model runs of anthropogenic CO_2. Further, we have applied these different sets of K_{ap} in a global box-diffusion model to calculate the uptake of anthropogenic CO_2 and of bomb ^{14}C. We found good agreement between K_{ap} derived from the 3-D model's radiocarbon and anthropogenic CO_2 distributions. Also, for our calculated uptake of bomb ^{14}C and anthropogenic CO_2, the GCM results agree well with those from our global box-diffusion (B-D) models.

Of general concern is the large difference between eddy diffusion coefficients used in models versus those measured in the real ocean. Diffusivity coefficients commonly used in box-diffusion type models are roughly 10 times larger than vertical diffusivities estimated for local mixing processes. We discuss here how these discrepancies arise: the magnitude of the diffusivity coefficient depends upon the processes being parameterized, which differ greatly as a function of the spatial scale involved.

This paper is organized as follows. Section 2 briefly describes the models, the simulations, and the impact of neglecting carbon transport by organic material. Section 3 details the eddy diffusion approach and the calculation of K_{ap}. For the results, we (1) compare the latitudinal distributions of different tracers, (2) assess global tracer transport in the vertical as due to advection, diffusion, and convection, (3) determine K_{ap} for each of these transport processes, (4) implant sets of total K_{ap} in the B-D model to simulate the uptake of radiocarbon and anthropogenic CO_2, and (5) analyze how K_{ap} differ regionally. Following the discussion, an appendix offers some of the finer details as to how we calculated K_{ap} from 3-D model results.

2. Model Descriptions

2.1. 3-D Model and Simulations

We used output from the GFDL 3-D model of Toggweiler et al. [1989a, b], a primitive equation model based on earlier work by Bryan [1969, 1979] and Bryan and Lewis [1979]. This 3-D model has twelve vertical layers, a north-south resolution of 4.5°, and an east-west resolution of 3.75°. Tracers are transported by advection, convection, and explicit eddy diffusion. Toggweiler et al. [1989a] computed the velocity fields by solving the

equations of motion and continuity, as well as conservation of salinity, temperature, and state. The GFDL model also uses the convective adjustment approach; that is, it homogenizes adjacent layers that are unstable with respect to one other. Explicit vertical eddy diffusivity varies smoothly between 0.3 cm^2 s^{-1} in the upper kilometer and 1.3 cm^2 s^{-1} in the deepest layer, whereas explicit horizontal eddy diffusivity decreases from 1.0 to 0.5×10^7 cm^2 s^{-1} from surface to bottom. For our studies of the transport of temperature in the GFDL GCM, we used the resulting stationary circulation and tracer fields from Toggweiler et al.'s [1989a] nonseasonal, prognostic, world-ocean model (version P).

For other tracers, we used an off-line version of the same model, thereby allowing more efficient use of computing resources. The off-line model is driven by time-averaged fields of advection and convection, saved from the on-line model ([Toggweiler et al., 1989a], prognostic version P) while running it an additional 55 years beyond equilibrium [Najjar, 1990]. The off-line model employs the convective index representing the fraction of total passes through the convection routine of the on-line model. For practical reasons, off-line convection is specified to never occur if the convective index is between 0 and 1/3, to pass once per time step through the convection routine if the index is between 1/3 and 2/3, or to pass twice per time step if the convective index is between 2/3 and 1. As such, off-line convection may not always be representative of that occurring in the on-line model. For anthropogenic CO_2, we used off-line results from the standard simulation of Sarmiento et al. [1992, simulation A1.1]. For bomb ^{14}C, we made a new simulation in the same 3-D off-line model because it was not possible to reconstruct the convective transport from the results stored for the on-line bomb ^{14}C runs of Toggweiler et al. [1989b]. In any case, comparison here between simulations for bomb ^{14}C and anthropogenic CO_2 is consistent since both simulations were made off-line in the same model.

We now turn to the geochemical models used for anthropogenic CO_2 and ^{14}C. The following equation

$$\frac{\partial C}{\partial t} = \text{advection} + \text{diffusion} + \text{convection} - \lambda C \tag{2}$$

describes tracer transport, with the first three terms on the right-hand side (advection, turbulent diffusion, and convection, respectively), all predicted by the dynamic 3-D model. The fourth term represents radioactive decay and is applicable here only for ^{14}C ($t_{1/2} = 5730$ years). In addition to equation (2), one must consider the surface boundary condition, the net air-sea tracer flux, which is the product of the difference between the atmosphere and surface ocean tracer concentrations and the gas exchange coefficient. The latter is assumed for the 3-D simulations to be a linear function of wind speed [Broecker et al., 1985; Esbensen and Kushnir, 1981] and of sea ice coverage. The gas

exchange coefficient, based on wind speed only, is multiplied by the observed annual average fractional area of each grid box which remains ice free [*Walsh*, 1978; *Zwally et al.*, 1983].

For anthropogenic CO_2, *Sarmiento et al.* [1992] used a perturbation approach, which relates changes in oceanic pCO_2 to changes in oceanic ΣCO_2, thereby simplifying the simulation. With the perturbation approach and its implied steady state assumption, it is not necessary to run simulations to equilibrium beforehand. Perturbation CO_2 simulations begin at the onset of the industrial revolution. Levels of atmospheric pCO_2 derive from a spline fit to the data [*Neftel et al.*, 1985; *Friedli et al.*, 1986; *Keeling et al.*, 1989].

For ^{14}C, *Toggweiler et al.* [1989a, b] used the fractionation corrected $^{14}C/^{12}C$ ratio [e.g., *Bolin*, 1981] as a tracer. Although $\Delta^{14}C$ is a ratio, in the context of this paper, it is employed as a ^{14}C concentration because model runs here explicitly avoid simulating fractionation. For natural ^{14}C, atmospheric ^{14}C concentration was prescribed at a fixed $\Delta^{14}C$ level of $0°/_{oo}$; for bomb ^{14}C, the atmospheric record was prescribed according to observations.

2.2. Box Model

To evaluate the K_{ap} derived from the 3-D model in the context of a simple model, we constructed a box-diffusion (B-D) model [*Oeschger et al.*, 1975] having the same vertical resolution as the 3-D model, that is, an ocean represented by 12 homogeneously mixed layers whose thicknesses increase smoothly from 51 m at the surface to 866 m at depth. Vertical tracer fluxes in the B-D model were computed while using the K_{ap} derived from the 3-D model. We calculated vertical gradients and fluxes in a manner consistent with the centered finite difference scheme used in the 3-D GFDL model [*Bryan*, 1969]. Thus exchange between the top two layers was calculated in the same way as for deeper layers.

Solving the diffusion equations by applying the GFDL model's first-order numerical scheme [see *Yin and Fung*, 1991] and its low vertical resolution yields substantially different results than applying the numerical approach used by *Oeschger et al.* [1975]. The latter is second-order accurate and has much finer vertical resolution. Thus diffusivities would have to be different for the two versions to obtain the same results. While using the same diffusivities in both versions, we found predicted uptake of anthropogenic CO_2 to differ by up to 25%.

We calculated tracer fluxes between atmosphere and ocean using a global-average value for the gas transfer coefficient. Ice cover was not considered in the B-D model, whereas it impedes gas transfer in the 3-D model. Note, however, that global CO_2 uptake in 3-D simulations with ice cover versus those without showed only slight differences. The B-D model's ocean surface area was set to $3.62 \times 10^{14} m^2$. With this B-D model, we ran simulations analogous to the standard experiments of *Sarmiento et al.* [1992] and *Toggweiler et al.*

[1989a, b]. We used the same perturbation approach as Sarmiento et al., as well as their global average gas exchange rate ($17.9 \, mol \, m^{-2} \, yr^{-1}$ at 275 ppm) to calculate the uptake of CO_2. Likewise for bomb ^{14}C, we patterned our B-D model simulation after the standard 3-D simulation of *Toggweiler et al.* [1989b], whose global average gas exchange rate was $16.6 \, mol \, C \, m^{-2} \, yr^{-1}$, constant in time. For comparison purposes, we followed Toggweiler et al. who neglect the increase in atmospheric carbon inventory and the invasion of anthropogenic CO_2 into the ocean for all simulations of bomb ^{14}C.

2.3. Neglect of Transport by Organic Material

In addition to ocean currents, convection, and turbulence, oceanic carbon is transported by the cycling of particulate and dissolved organic matter, as produced and consumed by marine organisms. The downward flux of biogenic material leaving the surface ocean and its subsequent remineralization at depth causes CO_2 concentration to be higher in the deep ocean relative to surface waters. Yet such transport was not included in the models described above because related changes in $^{14}C/^{12}C$ are relatively small. In the case of natural ^{14}C, where equilibrium between atmosphere and ocean has been established, it is the ratio of ^{14}C to ^{12}C in a water sample that is important. Both ^{14}C and ^{12}C are fixed into biogenic material in the same ratio (corrected for fractionation) as found in surface waters; subsequent remineralization of organic material increases both the ^{14}C and ^{12}C concentration. Thus the effect of biological transport on the $^{14}C/^{12}C$ ratio is relatively small. Any error introduced by ignoring the biological carbon transport is less than 10% of the natural $\Delta^{14}C$ signal produced by ocean circulation and radioactive decay [*Fiadeiro*, 1982].

As for bomb ^{14}C, its downward transport due to biological cycling corresponds to the product of new production (i.e., the flux of organic material leaving the mixed layer) times the bomb-^{14}C concentration in this organic material. The latter is approximately equal to the inorganic bomb-^{14}C concentration in surface waters. Levels of bomb ^{14}C in the surface ocean are known reasonably well. For new production, however, there exists a wide range of estimates: 4 Gt C yr^{-1} from *Eppley and Peterson* [1979], 6 Gt C yr^{-1} from *Berger et al.* [1987], 20 Gt C yr^{-1} from *Packard et al.* [1988], 7–13 Gt C yr^{-1} from *Najjar* [1992], 8.5 Gt C yr^{-1} from *Kurz and Maier-Reimer* [1993], and 19 Gt C yr^{-1} from *Keeling and Shertz* [1992].

To estimate the associated errors, we multiplied the HILDA model's time-integrated surface ratio of bomb ^{14}C [*Siegenthaler and Joos*, 1992] times a global export production of 10 Gt C yr^{-1}. Up to 1974, during the Geochemical Ocean Sections Survey (GEOSECS), we found a downward transport of 9×10^{26} atoms m^{-2}, roughly 3% of the observed global bomb-^{14}C inventory of 300×10^{26} atoms m^{-2} [*Broecker et al.*, 1985,

1995]. Such an effect is relatively small, particularly when compared to the uncertainties of roughly $\pm 10\%$ associated with current estimates of the bomb-^{14}C inventory [*Broecker et al.*, 1995; *Joos*, 1994]. Thus for Δ^{14}C, transport via biogenic material cycling plays a minor role and can be neglected.

For CO_2, the perturbation approach used here incorporates the steady state assumption for the natural carbon cycle. With this fundamental assumption, the ocean's biological fluxes are assumed not to have changed since preindustrial times. Strong support that such an assumption is valid when modeling atmospheric CO_2 comes from the roughly constant pCO_2 recorded in ice cores for at least 800 years prior the beginning of the industrial revolution as well as little evidence pointing to recent dramatic changes in ocean circulation and biology [e.g., *Siegenthaler and Sarmiento*, 1993]. Furthermore, model sensitivity studies show that large perturbations to the ocean's biological particle flux would be necessary if the atmospheric CO_2 concentration were to be altered substantially [e.g., *Joos et al.*, 1991]. In summary, it appears reasonable to neglect biological transport for simulations spanning the historical CO_2 transient.

3. Analysis

3.1. Turbulent Transport and the Eddy Diffusion Approach

Before discussing analysis of 3-D model results, let us first recall the concept of eddy diffusion [e.g., *Newell*, 1963; *Peixoto and Oort*, 1992]. Turbulent diffusion can be described as a flow varying in time and space by separating both the velocity $v(t, x)$ and the concentration $c(t, x)$ into averages (over time and space) and the remainder which fluctuates. The time- and space-averaged flux **f** per unit area and per unit time is then

$$
\begin{aligned}
\mathbf{f} &= \langle \overline{\mathbf{v} \cdot c} \rangle \\
&= \langle \overline{\mathbf{v}} \rangle \cdot \langle \overline{c} \rangle + \langle \overline{\mathbf{v}}(x)^* \cdot \overline{c}(x)^* \rangle \\
&\quad + \langle \mathbf{v}'(t, x) \cdot c'(t, x) \rangle.
\end{aligned} \tag{3}
$$

Here, the overbar indicates the average over time, the prime represents the temporal fluctuation, the angle brackets denote the spatial mean, and the asterisk indicates the spatial fluctuation. Thus the average flux through an arbitrary area during an arbitrary time interval consists of transport by the mean advection $\langle \overline{\mathbf{v}} \rangle$, transport by standing eddies $(\overline{\mathbf{v}}(x)^*$, that is, by the spatial fluctuations of the time-averaged circulation), and transport by transient eddies.

The eddy diffusion approach assumes that the turbulent flux (last two terms in equation (3)) is proportional to the mean tracer gradient. In three dimensions, the turbulent flux is then the product of the tracer gradient and the tensor **K**, a matrix consisting of the eddy diffusivity coefficients [e.g., *Redi*, 1982]. With the eddy

diffusion assumption, one can now describe the average flux **f** in direction of the unit vector **n** as

$$
\mathbf{f} = \langle \overline{\mathbf{v}} \rangle \cdot \langle \overline{c} \rangle - [\mathbf{n} \cdot \mathbf{K} \cdot \nabla \langle \overline{c} \rangle] \cdot \mathbf{n}, \tag{4}
$$

which is equivalent to equation (1) but written for three dimensions. As for eddy diffusion coefficients (i.e., the elements of the **K** matrix), definitions vary between models. In the simplest cases, coefficients are assumed constant [e.g., *Oeschger et al.*, 1975]; in more complex cases, they are calculated using sophisticated models for production, transport, and dissipation of turbulent kinetic energy [e.g., Gaspar et al., 1990].

By representing equation (4) in a coordinate system in which **K** is diagonal, we can express the diagonal element of **K** as a function of averaged quantities. For example, when considering the flux f_z normal to a horizontal area, we obtain for such a special case the vertical eddy diffusion coefficient

$$
K_z = \frac{\langle \overline{v_z} \rangle \cdot \langle \overline{c} \rangle - f_z}{\partial \langle \overline{c} \rangle / \partial z}, \tag{5}
$$

where $\langle \overline{v_z} \rangle$ is the spatially and temporally averaged vertical velocity.

3.2. Calculating K_{ap} From the 3-D Model

To study the parameterization of large scale mixing by eddy diffusion, we used the same approach to determine advective fluxes as in earlier work by *Siegenthaler and Joos* [1992]; however, we extended this prior analysis by also considering, independently, the fluxes due to the 3-D model's convection and explicit diffusion. We computed the 3-D model's K_{ap} by horizontally averaging its concentration, flux, and velocity fields over a large ocean area and evaluated these averaged quantities in an equation analog to equation (5). The total K_{ap} were split into the sum of three components, K_{adv}, K_{conv}, and K_{diff}, defined by the 3-D model's advective, diffusive, and convective tracer fluxes, as described in the appendix.

When calculating K_{ap} by dividing the tracer flux by the vertical tracer gradient as in equation (5), results became unreliable when tracer gradients differed little from zero, which in part arises from the finite numerical precision necessary for both the model simulation and its analysis. One can check if such problems arise here, however, because that component of K_{ap} calculated from the explicit diffusive 3-D flux, K_{diff}, must equal the 3-D model's prescribed vertical diffusion coefficient. When they differed by more than 2%, we flagged the tracer gradient as numerically insignificant and did not use corresponding results. Occasionally, vertically adjacent values were also rejected based on a more detailed analysis.

For the calculation of the advective component, K_{adv}, temporal fluctuations (last term in equation (3)) were neglected (see appendix); therefore the component of

K_{ap} calculated from the 3-D's advective flux, K_{adv}, corresponds to

$$K_{adv} = \frac{\langle w^* c^* \rangle}{\partial \langle c \rangle / \partial z},$$ (6)

where w^* and c^* represent the spatial deviations of the vertical velocity and concentration in the 3-D model, relative to values averaged over a given horizontal area. This net advection by large overturning cells, which is resolved in the 3-D model, can only be taken into account via diffusion in the box model. Examples for such cells are the wind-driven overturning cells at the equator and the so-called Deacon cell in the Southern Ocean (see Figure 1).

Since K_{adv} effectively represents large-scale overturning (equation (6)), it seemed most appropriate to determine its value (and thus corresponding values of K_{diff}, K_{conv}, and K_{ap}) only in regions that include at least one such cell. For the global analysis, this presented no problem. For a regional analysis, we selected characteristic regions by using the meridional stream function (Figure 1) as a guide; to refine selection, we also relied on the depth-integrated, squared, northward water transport versus latitude (not shown). With minimum latitudinal water exchange near 31°S and 27°N in all ocean basins (Figure 1), we chose three distinct regions to be presented later in section 4.6: 90°S–90°N (the global ocean), 90°S–31°S (where strong convection dominates in the GFDL model and where there exists a large overturning cell), and 31°S–27°N (a nonconvective region having two wind-driven cells, one on each side of the equator). The exact latitudinal boundaries were not critical to this analysis; that is, calculated K_{ap} changed little when these boundaries were moved several degrees. As might be expected, attempts to use equation (6) on latitudinal bands of only one to two grid boxes (4.5° per band) produced K_{adv} which vary erratically with latitude.

4. Results

4.1. Surface Tracer Distributions in the 3-D Model

Because tracers considered here have different boundary conditions, their concentrations may also vary differently in space and time. Just how tracers vary in this regard is key to understanding differences in downward tracer transport. Here we first discuss spatial variability of different tracers. Then we address temporal variations.

It follows from equation (6) and the tracer-independent advective field that the K_{adv} for two tracers will be similar when both exhibit similar spatial distributions. With like distributions, downward transport carries like concentrations. For more insight, we compared normalized zonally averaged tracer distributions, c_{norm}, in the surface layer of the global ocean. Each tracer concentration c was normalized by using a scale which assigns a value of zero to the global average surface concentration, $\langle c_s \rangle$, and a value of -1 to a representative deep ocean concentration, $\langle c_d \rangle$:

$$c_{norm} = \frac{c - \langle c_s \rangle}{\langle c_s \rangle - \langle c_d \rangle},$$ (7)

Thereby we were able to measure the latitudinal variations at the surface, in units of the tracer's global average surface-to-deep concentration difference, which corresponds to a normalization with respect to the surface-
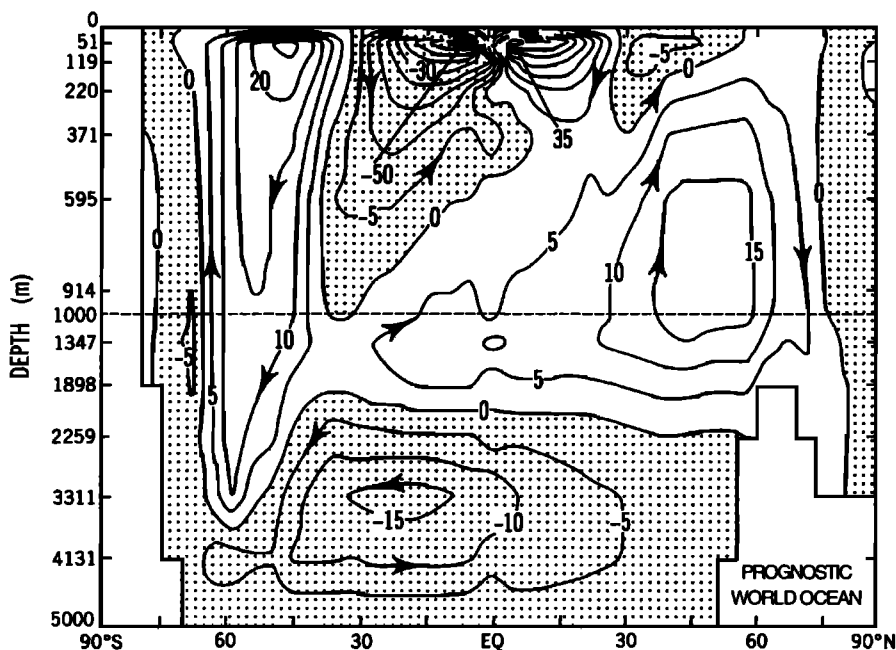

Figure 1. Meridional overturning for the global ocean.

to-deep gradient, that is, the denominator of equation (5) and equation (6).

As shown in Figure 2, normalized surface distributions were roughly similar for anthropogenic CO_2, natural ^{14}C, and bomb [14]C. All three tracers exhibited lows near the equator (due to upwelling of tracer-impoverished water) and highs in the subtropical gyres (after substantial air-to-sea invasion of tracer). Other similarities included the sharp decline between the subtropical gyres and high-latitude regions, where surface-to-deep mixing is enhanced. Although normalized surface concentrations between 50° S and 50° N (which comprises 80% of the world ocean's surface area) remained fairly close to the basin-wide averages, surface water concentrations increased between the equator and the subtropical gyres at different rates. These differences arose largely because during surface water transport toward the midgyre regions (Figure 1), each tracer equilibrated at different rates with the atmosphere. Differences between equator and midgyre concentrations were most pronounced for bomb ^{14}C because of its large air-sea gradient as well as the long time ($\sim$10 years) required for perturbations of the ^{14}C/^{12}C ratio to equilibrate with surface waters. Anthropogenic CO_2's equilibration time is about 10 times faster; natural [14]C's steady state input and its smaller air-sea difference made its surface distribution between 50° S and 50° N much more like that for anthropogenic CO_2.

Temperature showed a completely different distribution. In mid and low latitudes, which cover most of the ocean's surface, temperature varied over almost the entire range of values found in the ocean. Although informative, the above analysis of the spatial tracer distributions is limited. For example, gradients along isopycnal surfaces were not considered. Nevertheless, one might anticipate that K_{ap} profiles for ^{14}C and anthropogenic CO_2 would be similar, whereas the temperature profile would be substantially different. As shown below, this is indeed the case.

4.2. Tracer Fluxes in the 3-D Model

To further compare tracers, we separated downward tracer transport into components due to advection, convection, and explicit diffusion. Figure 3 shows the 3-D model's globally averaged downward flux for anthropogenic CO_2 (1986), natural ^{14}C, bomb ^{14}C in 1974, and temperature. Downward fluxes decreased with depth for the two transient tracers. The radioactive decay of natural ^{14}C dictates that its globally averaged downward flux must also decrease with depth because at steady state, net supply must balance decay in each layer. A conservative tracer, such as temperature, must have zero globally averaged vertical flux at all depth levels.

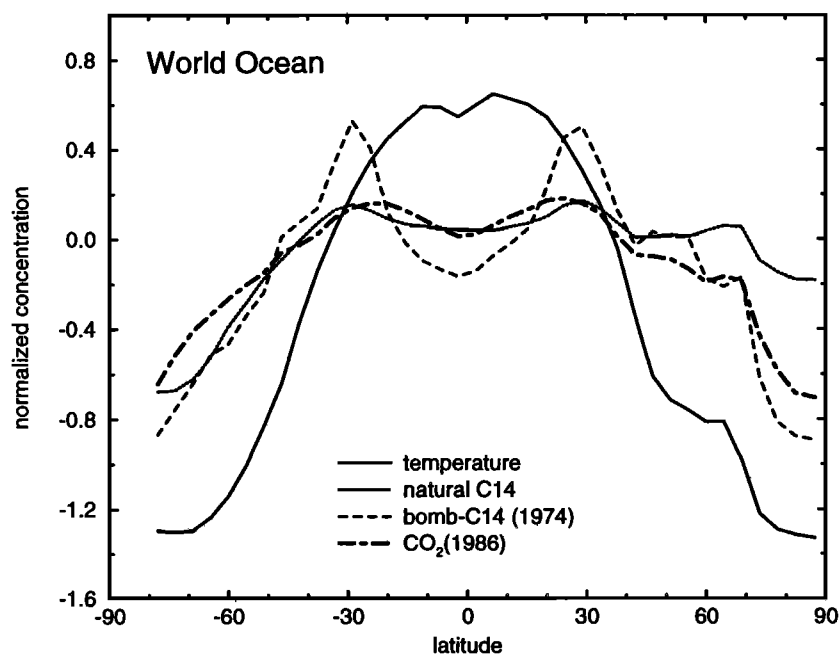Downward transport of anthropogenic CO_2 across the upper layers of the 3-D model was split about equally

Figure 2. Zonal-average surface values of temperature (solid), preindustrial [14]C (dotted), bomb-produced [14]C (dashed), and anthropogenic CO_2 (dash-dotted) as simulated in the GFDL 3-D model versus latitude. For consistency, results from each tracer are given on a normalized scale ranging from -1 (for representative deep-sea values) to 0 (for the basin-wide average of the surface concentration). For the -1 end of the normalization, we take deep-ocean bomb ^{14}C and anthropogenic CO_2 at zero concentration, and for temperature and natural ^{14}C, we take their average concentrations at 2200 m.
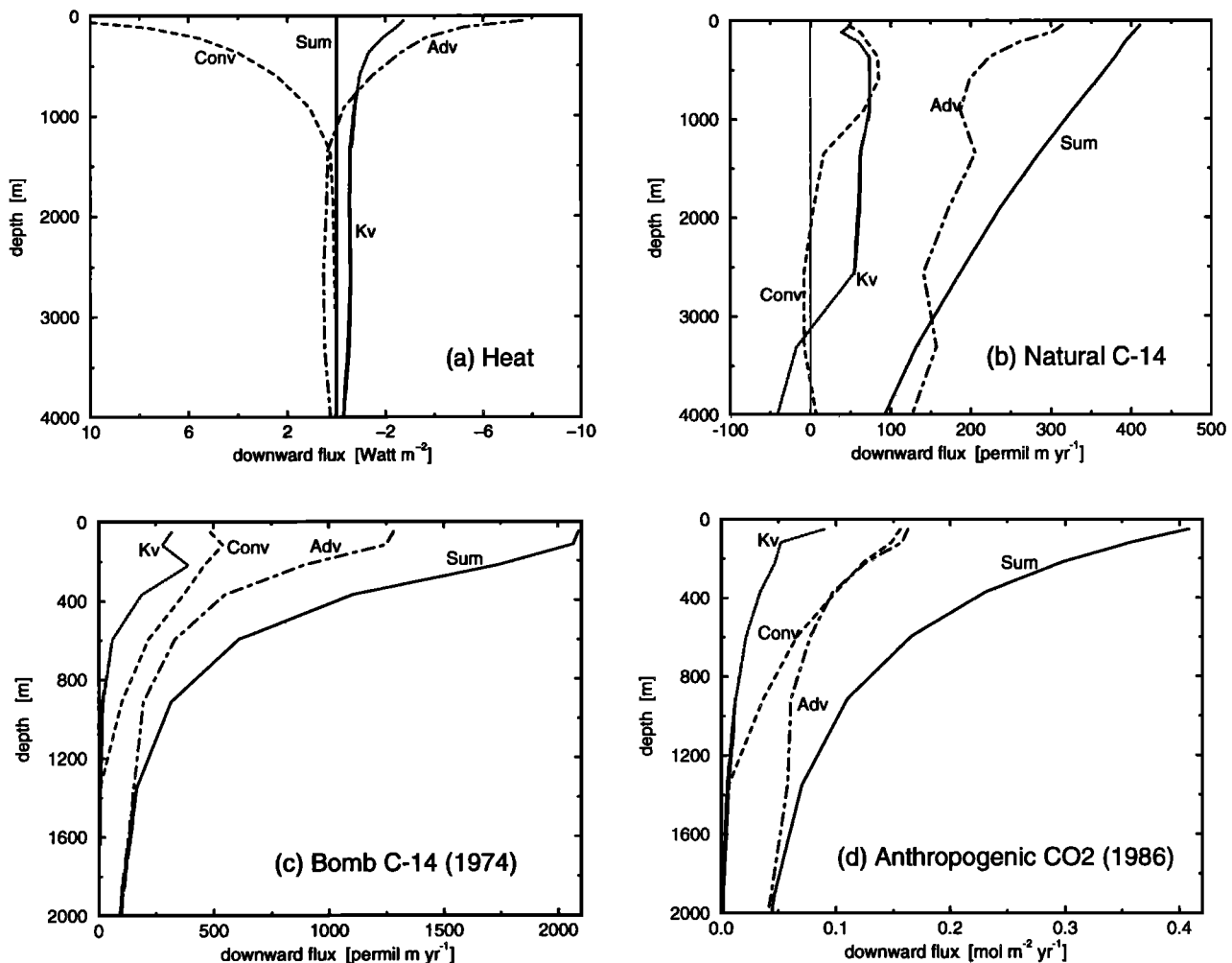
Figure 3. Downward transport of (a) heat, (b) natural ^{14}C, (c) bomb ^{14}C (1974), and (d) anthropogenic CO_2 (1986) versus depth for the global ocean as simulated in the GFDL 3-D model. Transport processes are separated into components due to advection (dash-dotted), convection (dashed), explicit diffusion (dotted), and the sum of all three processes (solid).

between advection and convection. Advection dominated across deeper layers. Vertical transport by explicit diffusion was relatively small throughout the water column. For CO_2, the relative importance of these three transport mechanisms did not change substantially with time.

The situation for bomb ^{14}C was different (Figure 4). Convection and advection contributed about equally to the downward flux of bomb ^{14}C before 1963, but unlike the case for anthropogenic CO_2, transport to depth by explicit diffusion was also substantial. After 1963, most of the model's downward flux of bomb ^{14}C derived from advection.

Variations in the relative importance of the different transport processes were linked to the history of anthropogenic CO_2 and bomb ^{14}C (Figure 5). In upper layers, convection was of equal or higher importance than advection during the rise in surface CO_2 and ^{14}C (compare Figures 3d, 4a, and 5). Because the 3-D model's explicit diffusion and convection act on a local scale, both these

processes tended to decrease the vertical tracer gradient. Thus their efficiencies for transporting tracers to depth decreased with time because resupply from the atmosphere could not keep pace. In contrast to convection, the advective transport did not depend on local vertical gradients, but on the concentration differences between upwelling and downwelling regions. Thus, for the large overturning cells shown in Figure 1, net advective downward flux depended on the concentration difference of horizontally distant regions. In upwelling regions, ^{14}C concentrations remained low because there the slow influx of bomb ^{14}C from the atmosphere could not keep up with the renewal from below by waters impoverished in bomb ^{14}C. On the other hand, continuous enrichment by air-sea exchange of surface waters during their transit from upwelling regions toward the midlatitude gyres resulted in relatively high gyre concentrations. Thus one finds a local minimum around the equator and the maximum in the midlatitudes (Figure 2).
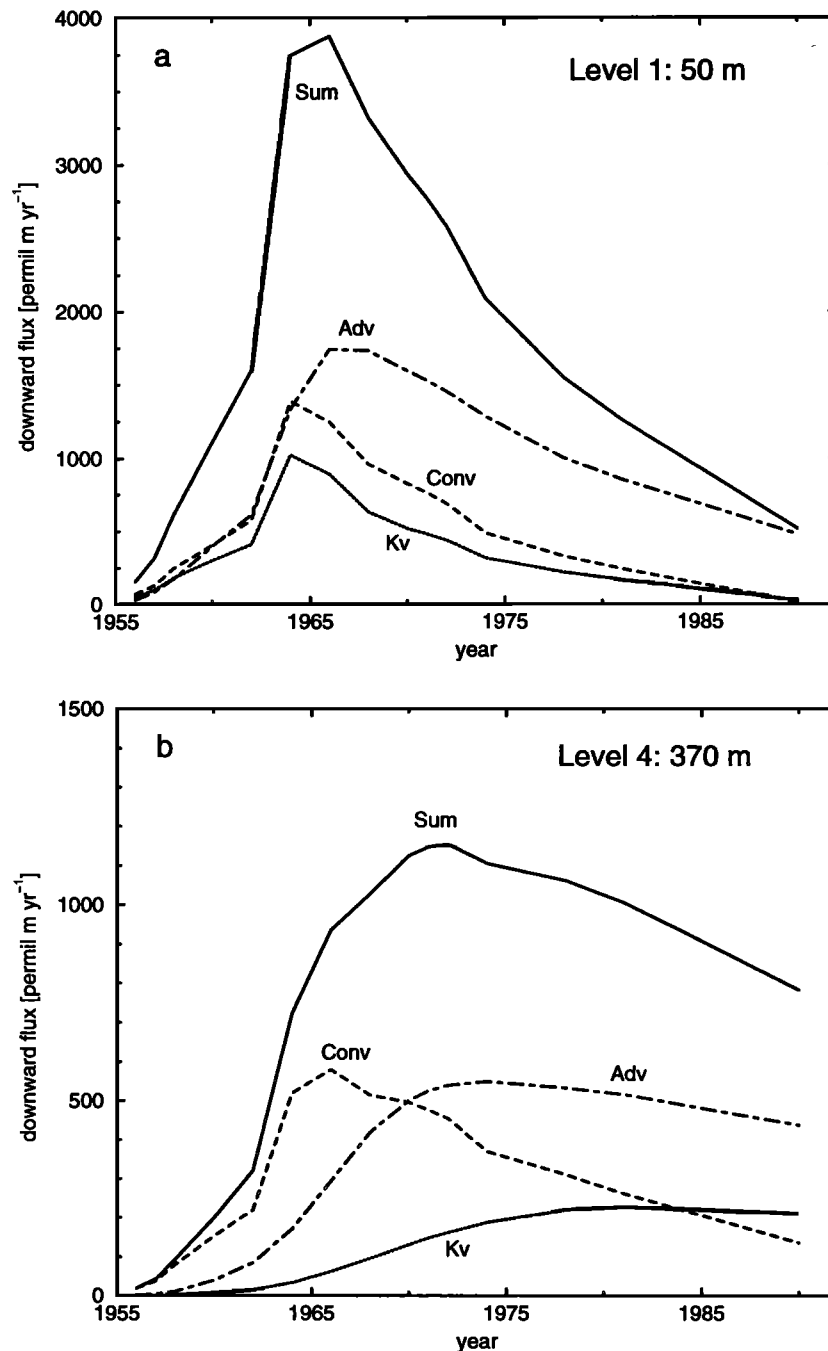
Figure 4. Downward transport of bomb ^{14}C versus time for global ocean as simulated in the GFDL 3-D model at a depth of (a) 50 m and (b) 370 m. Note different vertical scale. Line patterns are as in Figure 3.

The main processes responsible for the global distribution of natural ^{14}C were thermohaline overturning and radioactive decay. Convective transport played a minor role (Figure 3b) because the timescale governing convection is much shorter than the half-life of ^{14}C. Also, ^{14}C's air-sea equilibration time is slow when compared to the residence time of high-latitude surface waters. Thus, in regions of convection, the depth distribution of natural ^{14}C was nearly homogeneous. Therefore convection had relatively little effect on the global mean vertical distribution of natural ^{14}C (Figure 3b).

The temperature distribution was controlled by a more subtle balance between convection, advection, and explicit diffusion (Figure 3a). Vertical explicit diffusion must transport heat from surface to depth because the ocean's average temperature decreases with depth. In the deep ocean, the global downward transport of heat by diffusion was balanced primarily by upward heat
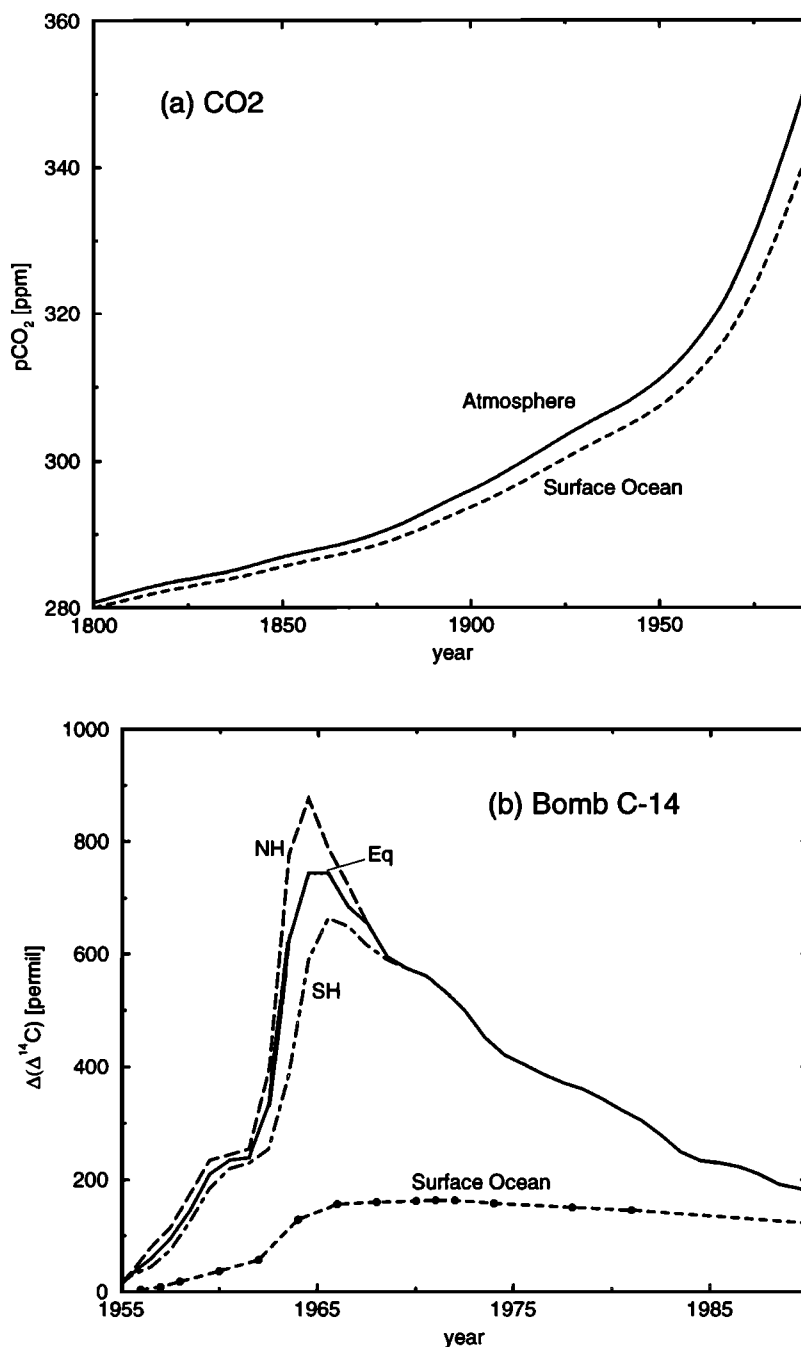
Figure 5. (a) History of atmospheric CO_2 as revealed by ice core analysis and direct atmospheric measurements and of the CO_2 partial pressure in surface water as simulated with the HILDA model. (b) History of bomb-produced ^{14}C concentration as observed for southern hemisphere (dash-dotted), Equatorial (solid), and northern hemisphere (long-dashed) air and as simulated for the global surface ocean (dashed line [*Toggweiler et al.*, 1989b]. Solid circles denote the years for which model output is available.

fluxes due to advection, with a smaller contribution by convection. Advection was also important in the thermocline, but opposite in sign (downward). We found by analyzing regional heat fluxes that heat was advected into the upper thermocline by the wind-driven overturning cells in mid and low latitudes, and advection in the high latitudes sent heat from the surface to the deeper layers. This large advective downward heat flux in the

top 1000 m was mainly balanced by convective cooling in the high latitudes.

Transport pathways for the four tracers considered here (temperature, anthropogenic CO_2, natural ^{14}C, and bomb ^{14}C) were remarkably different. Thus one cannot assume a priori that these tracers have identical sets of K_{ap}, nor that their K_{ap} are constant through time. The net global downward flux of a conservative

tracer at steady state is zero; thus, derived K_{ap} must be zero as well. Therefore distributions of conservative tracers, such as temperature and salt, are not appropriate tracers for deriving diffusion coefficients for nonconservative or transient tracers. Furthermore, the essential assumption of the eddy diffusion concept, that is, that a tracer's gradient drives its flux, did not hold for the global ocean temperature distribution.

4.3. Magnitude and Structure of Global K_{ap}

Figure 6a shows K_{ap} determined for the global ocean with 3-D model results from simulations of natural ^{14}C, bomb ^{14}C (in 1974), and anthropogenic CO_2 (in 1986). Results for anthropogenic CO_2 and bomb ^{14}C are displayed only in the upper layers because K_{ap} are meaningless when calculated far below a tracer's penetration depth. Resulting K_{ap} for all tracers ranged between 4000 and 10,000 m^2 yr^{-1}; however, vertical profiles differed considerably. The highest values for natural ^{14}C were in the top three layers, whereas K_{ap} increased with depth for anthropogenic CO_2. Our K_{ap} were essentially

bracketed by the depth-constant diffusivities found by *Oeschger et al.* [1975] and *Siegenthaler and Oeschger* [1987], who fit their B-D model to the observed natural ^{14}C (K=4000 m^2 yr^{-1}) and bomb-^{14}C (K=7100 m^2 yr^{-1}) distributions.

Though K_{ap} profiles for anthropogenic CO_2 changed little with time (Figure 7), those for bomb ^{14}C changed substantially. Tritium, another bomb tracer, also shows time variable K_{ap} [*Sarmiento*, 1983]. Figure 8 shows the temporal change of K_{ap} for bomb-^{14}C, as separated into advective, diffusive, and convective components for the top four layers. In the top three layers, K_{adv} was small at the beginning of the simulation but increased with time, whereas the reverse was true for deeper layers. For explanation, we recall that the apparent diffusivity depends on the correlation between the vertical velocity field and the tracer's concentration (equation(6)). When the run is initialized, K_{adv} was small because input of bomb ^{14}C was only slightly correlated with the vertical velocity field. The circulation tended to increase the correlation with time (and thus K_{adv}) by concentrating the bomb ^{14}C in downwelling areas. In deeper layers, the ^{14}C concentration and velocity fields were more strongly correlated from the beginning because most bomb ^{14}C is transported there by advection. Subsequent mixing by explicit diffusion smoothed the tracer field, and thus K_{adv} fell off.

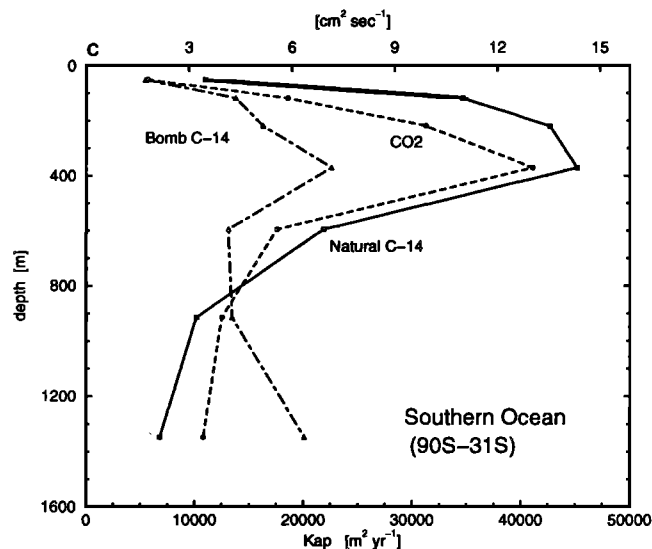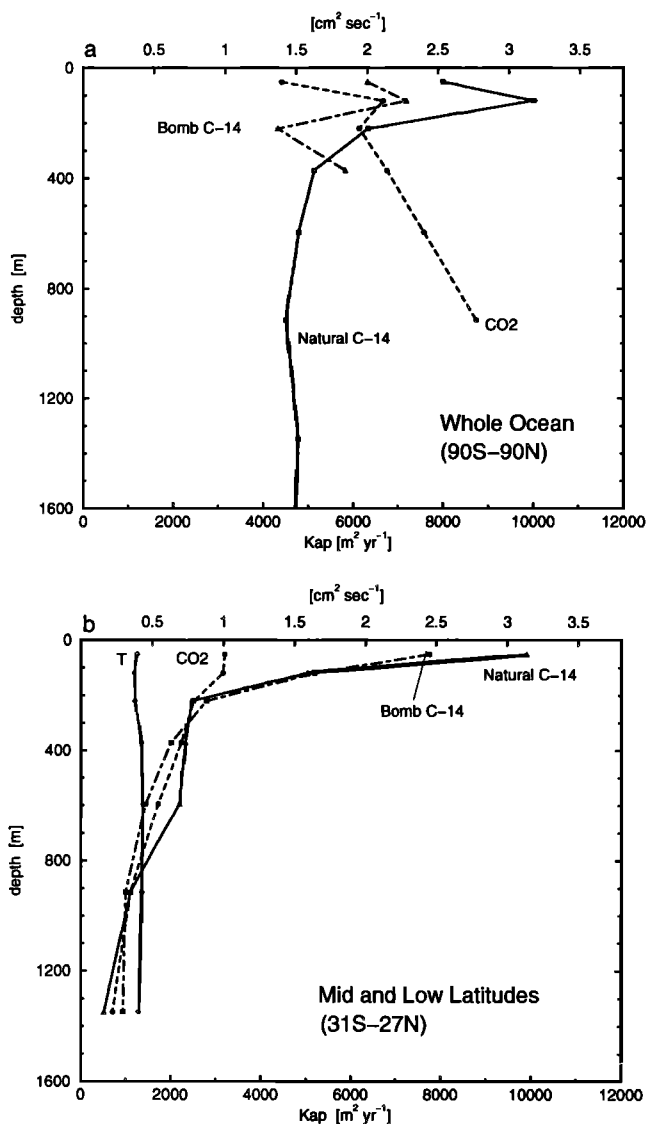Besides this temporal change in correlation between the vertical velocity and tracer fields, the vertical gra-

Figure 6. Apparent diffusivity coefficients versus depth as calculated from the results of the 3-D GFDL model simulations for anthropogenic CO_2 (dashed), natural ^{14}C (solid), bomb-produced ^{14}C (dash-dotted, 1974) and temperature (dotted). Results are given for (a) the global ocean, (b) the mid and low-latitude ocean (31°S and 27°N), and (c) the Southern Ocean (90°S-31°S). Temperature-derived values are shown only for mid and low latitudes (i.e., apparent diffusivities for temperature vanish when calculated over the global ocean; they are negative for the Southern Ocean).
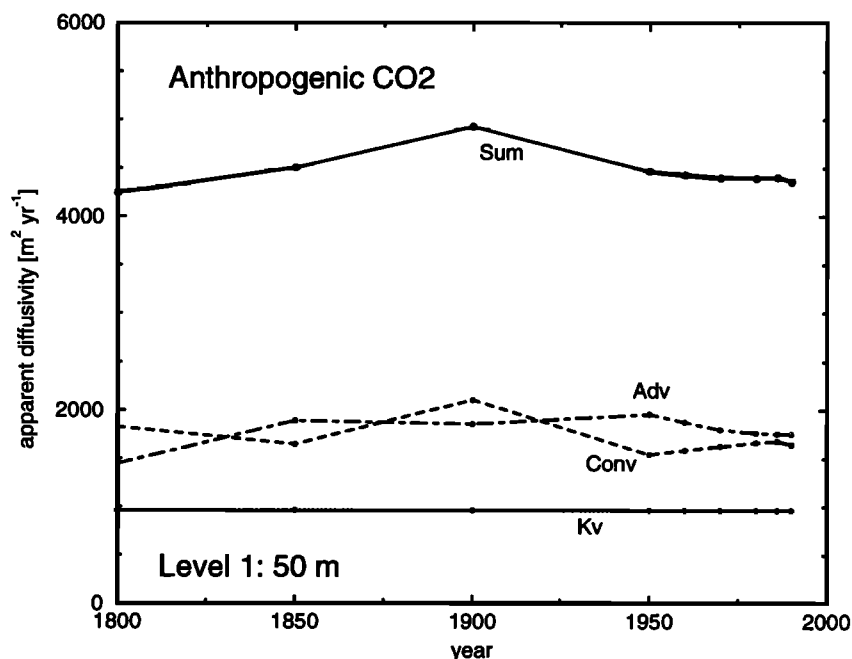
Figure 7. Apparent diffusivity coefficients versus time as calculated from results of 3-D GFDL simulations for anthropogenic CO_2. Transport processes are denoted in the same manner as in Figure 3.

dient decreased after 1964 across the top two levels and after 1970 in the third level; conversely, the gradient increased in deeper layers throughout the whole period. Thus the evolution in the gradient supported the increase with time of K_{adv} in the top layers and its decrease below.

As for the convective component K_{conv}, original values were high but leveled off in all but the surface layer, where they remained more or less constant until their notable decline after 1980. When convective transport was most noticeable, at the beginning of the simulation, globally averaged gradients were small. During that time, K_{conv} had to be large. Values of K_{conv} dropped off as the vertical ^{14}C gradient increased.

The total K_{ap} increased with time in the top two layers, but decreased with time below. In short, the assumption that diffusivities are time independent was not valid for bomb ^{14}C. Despite such large temporal changes, however, we show below that assuming time-independent K for box models has little impact when simulating global ocean uptake of anthropogenic CO_2, nor even upon global uptake of bomb ^{14}C.

4.4. Box-Model Simulations With K_{ap} From the 3-D Model

We have run B-D model simulations with the different sets of K_{ap} from the 3-D model. Simulations were forced with atmospheric histories of bomb ^{14}C and anthropogenic CO_2, just as in the 3-D model. The oceanic uptake of these two transient tracers was not identical because the main process limiting uptake is different

in each case: uptake of anthropogenic CO_2 is limited mainly by rates of surface-to-deep mixing, while bomb ^{14}C uptake (up through the period of GEOSECS) is limited primarily by ^{14}C's long air-sea equilibration time. Table 1 presents the bomb-^{14}C penetration depth (inventory/surface concentration [*Broecker et al.*, 1985], which is largely independent of the gas exchange rate. Thus the bomb-^{14}C penetration depth provides a better means to characterize surface-to-deep mixing in the ocean and serves as a better analog for oceanic uptake of anthropogenic CO_2.

We first investigated the sensitivity of transient tracer uptake to the magnitude of depth-independent diffusivities (Table 1, section A). A 33% decrease in K (from 6000 to 4000 m^2 yr^{-1}) resulted in a 16% drop in oceanic uptake of anthropogenic CO_2 and a 17% decline in the bomb-^{14}C penetration depth. A 33% increase (from 6000 to 8000 m^2 yr^{-1}) raised CO_2 uptake and bomb-^{14}C penetration depth by 13 and 14%, respectively. For the same 33% increase, however, the inventory of bomb ^{14}C rose by only 4%. As a general rule then, a relative increase in the B-D model's diffusivity (in this case constant with depth) resulted in less than half as much proportional rise in the penetration of bomb ^{14}C and anthropogenic CO_2.

Next, we explored the role of diffusivity variations with time and depth (Table 1, section B). Six different versions (B1-B6) of the global B-D model were used, each employing a separate, time invariant set of K_{ap} derived from 3-D model output. Specifically, the B-D runs used K_{ap} from 3-D output for natural ^{14}C (B1),
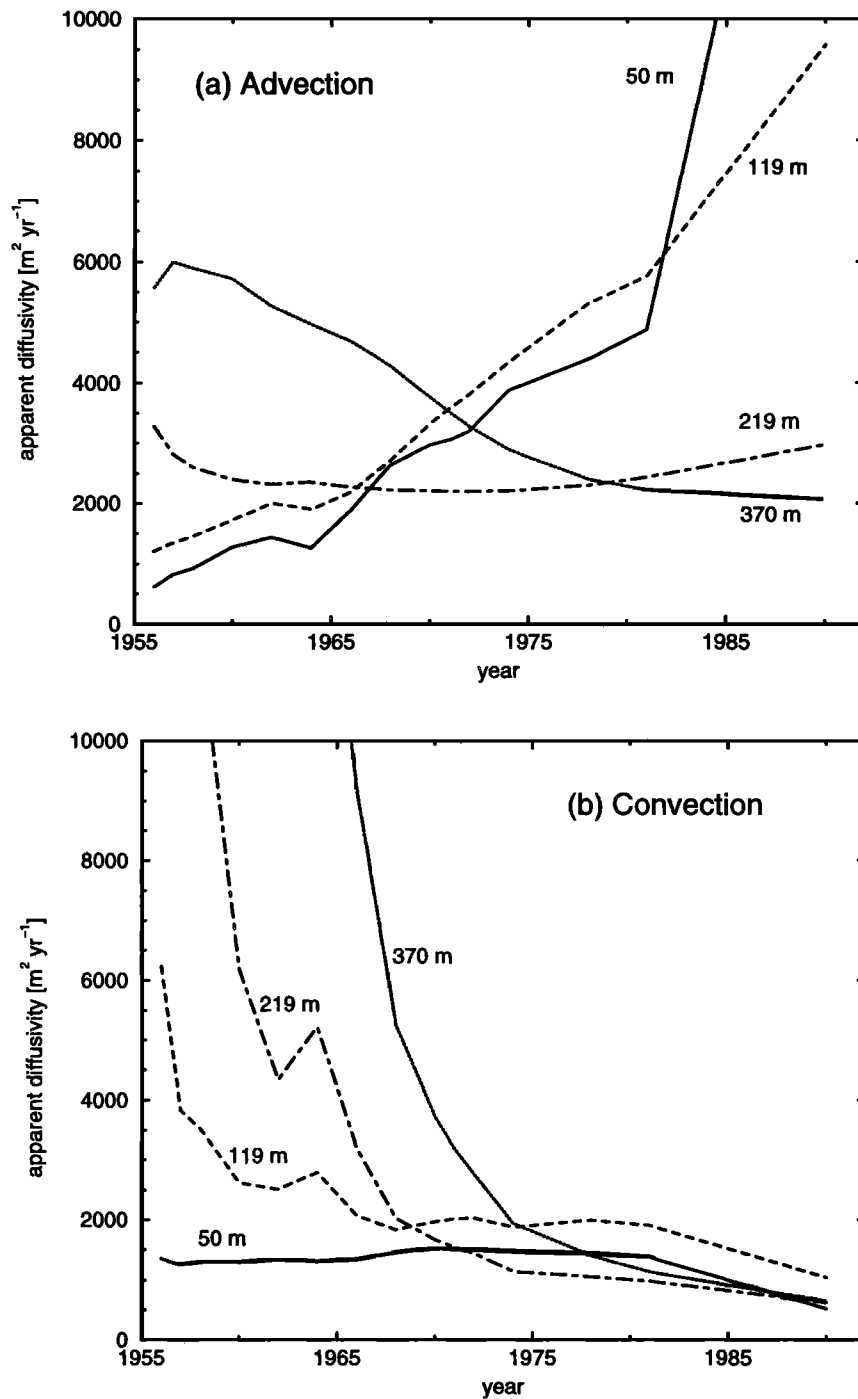
Figure 8. Apparent diffusivity coefficients versus time as calculated from results of 3-D GFDL simulations for bomb ^{14}C showing transport by (a) advection and (b) convection. The explicit vertical tracer diffusivity prescribed in the GCM is around 1000 m^2 yr^{-1}. Results are given for the upper four model layers.

bomb ^{14}C in 1970 (B2), 1974 (B3), and 1990 (B4), anthropogenic CO_2 (B5), and a combination of values derived from bomb ^{14}C (in 1970) plus natural ^{14}C (B6). Only in the top few layers was it possible to determine K_{ap} from the 3-D model's anthropogenic CO_2 and bomb-^{14}C distributions with adequate numerical precision (K_{diff} within 2% of the 3-D model's explicit diffusivity). Thus we extrapolated deep ocean values of K_{ap}

for B-D versions B2-B5 (see Table 2). As expected, the way in which K_{ap} are specified in deeper layers of the B-D model changed little the model results for the bomb-^{14}C uptake through the time of GEOSECS (1974); however, it did alter estimates of anthropogenic CO_2 uptake. Bomb-^{14}C observations are not sufficient in themselves to fully constrain downward mixing of anthropogenic CO_2 because the former has had less time

Table 1. Oceanic Uptake of Anthropogenic CO_2 and Bomb ^{14}C Predicted by the 3-D GFDL Model and the B-D Model

| | Uptake of Anthropogenic CO_2 | | Penetration Depth of Bomb Radiocarbon, m | |
	1980, Gt C yr^{-1}	1770-1980, Gt C	1974	1990
A: Box-Diffusion Model[a]				
A1 K=4000 m^2 yr^{-1}	1.51	85	254	458
A2 K=6000 m^2 yr^{-1}	1.80	101	306	551
A3 K=8000 m^2 yr^{-1}	2.03	115	350	623
B: Box-Diffusion Model[b]				
B1 K(natural ^{14}C)	1.86	103	327	560
B2 K(bomb ^{14}C, 1970)	1.84	104	291	565
B3 K(bomb ^{14}C, 1974)	1.84	104	293	545
B4 K(bomb ^{14}C, 1990)	1.86	101	331	527
B5 K(anthropogenic CO_2)	1.82	104	289	538
B6 K(bomb and natural ^{14}C)	1.69	95	284	517
C: 3-D Model[c]				
C1 *Sarmiento et al.* [1992]	1.65	92	-	-
C2 *Toggweiler et al.* [1989b]	-	-	292	523

Several versions of the B-D model are used, each having a different set of eddy diffusivity coefficients; see Table 2 for the explicit profiles used in versions B1-B6. The model's bomb-^{14}C penetration depth is calculated by dividing area-averaged bomb-^{14}C inventory (unit: ^{14}C-atoms m^{-2}) by bomb-^{14}C surface concentration (unit: ^{14}C-atoms m^{-3}) for both 1 January 1974 and mid-1990. The penetration depth characterizes oceanic mixing and is independent of gas exchange and the model's ocean surface area. GFDL, Geophysical Fluid Dynamics Laboratory; B-D, box-diffusion.

[a]Diffusivity K constant with depth.

[b]Diffusivities obtained by analyzing the 3-D model's tracer distribution for the global ocean (90°S-90°N).

[c]Global ocean, 90°S-90°N.

to invade deeper layers. Thus, ocean models are better calibrated when both natural and bomb ^{14}C are used simultaneously, that is, when mixing rates are derived from bomb ^{14}C in the upper ocean and natural ^{14}C at depth [*Siegenthaler and Joos*, 1992]. We followed an analogous approach for model version B6: we used the K_{ap} from the 3-D simulation for bomb ^{14}C (in 1970) for the top three layers , whereas for deeper layers, we used those from the simulation for natural ^{14}C. Table 1 also includes results from the 3-D model itself.

For the bomb-^{14}C penetration depth (evaluated in 1974), we found values between 284 and 293 m for the 3-D model itself and for four versions of the B-D model employing K_{ap} derived from output of 3-D model: B2, B3, B5, and B6. Penetration depths were about 10% deeper for the other two versions of the B-D model, that is, those for which K_{ap} were derived from 3-D simulations for natural ^{14}C (B1) and bomb ^{14}C at 1990 (B4). Table 1 also presents results for the penetration depth evaluated in 1990: relative differences are even less (within 8%) than are those evaluated in 1974. Concerning oceanic CO_2 uptake (in 1980), all six versions of the B-D model agreed to within 13% with the 3-D model. The closest agreement with the 3-D model's

CO_2 uptake (within 2%) was exhibited by version B6 (K_{ap} derived from both natural and bomb ^{14}C). All versions of the B-D model overestimated CO_2 uptake when compared with the 3-D model. Part of the reason is the B-D model's horizontal area that remains constant with depth (3.62 × 10^{14} m^2), whereas the 3-D's horizontal extension decreases from 3.55 × 10^{14} m^2 at surface to 3.47 × 10^{14} m^2 at 595 m, that is, about the penetration depth of anthropogenic CO_2 in 1990. Applying a rough geometry correction of 3% ((3.62-3.51)/3.62) reduces the differences between B-D and 3-D model to be equal or less than 10% . A more substantial difference for model versions B2–B5 is related to the extrapolation of shallow diffusivities to depth, which made deep diffusivities too high, as discussed below.

Figure 9 shows the globally averaged vertical profiles of natural ^{14}C, bomb ^{14}C, and anthropogenic CO_2, as obtained from the 3-D model and the different versions of the B-D model. In the upper layers, profiles agreed well for the two transient tracers (Figures 9b and 9c), although differences were not negligible between results of the 3-D model and B-D model version B1 (K_{ap} derived from natural ^{14}C). For deeper layers in B-D versions B2-B5, extrapolated diffusivities were too high,

Table 2. Apparent Diffusivity Coefficients as Calculated From the Distributions of Natural and Bomb ^{14}C, and Anthropogenic CO_2 in the GFDL/Princeton 3-D Ocean Model

Depth	Apparent Diffusivities, K_{ap}					
	Natural ^{14}C (B1)	Bomb ^{14}C 1970 (B2)	Bomb ^{14}C 1974 (B3)	Bomb ^{14}C 1990 (B4)	Anthropogenic CO_2 (B5)	Bomb and Natural ^{14}C (B6)
51	7997	5463	6308	19591	4404	5463
119	10006	6244	7179	11581	6659	6244
220	6328	4846	4319	4569	6130	4846
371	5123	8464	5819	3696	6751	5123
595	4782	8464	10017	5097	7580	4782
914	4496	8464	10017	5097	8736	4496
1347	4778	8464	10017	5097	8736	4778
1898	4625	8464	10017	5097	8736	4625
2559	4625	8464	10017	5097	8736	4625
3311	4625	8464	10017	5097	8736	4625
3800	4625	8464	10017	5097	8736	4625

Coefficients are given for the global ocean and are as used in versions B1-B6 of the B-D model (see text). Eddy diffusivities are in units of square meters per year; the depth at the bottom of each vertical layer in the 3-D and the B-D model is given in meters. Total depth of the B-D model is 3800 m. Eddy diffusivities in deep layers cannot be calculated from the 3-D tracer distributions, as gradients tends toward zero. These values are set to be equal to the value at the deepest layer for which calculation of diffusivity was numerically feasible.

when compared to the values found by analyzing the 3-D model's natural ^{14}C distribution (Table 1). Thus, relative to the 3-D model, too much ^{14}C (i.e., an excess of as much as $60°/_{oo}$) was produced in the deep ocean for these B-D model versions. The excess was much less ($10–25°/_{oo}$) when K_{ap} were derived from 3-D simulations for natural ^{14}C. Considering though, that the 3-D model resolves ocean topography, and that the maximum depth of the two models is different (5000 m versus 3800 m), one cannot expect very close agreement.

Overall, we found a reasonable accord between 3-D model results and the different versions of the B-D model. The excessive (10%) CO_2 uptake found for versions B2-B5 was due to diffusivities that were too
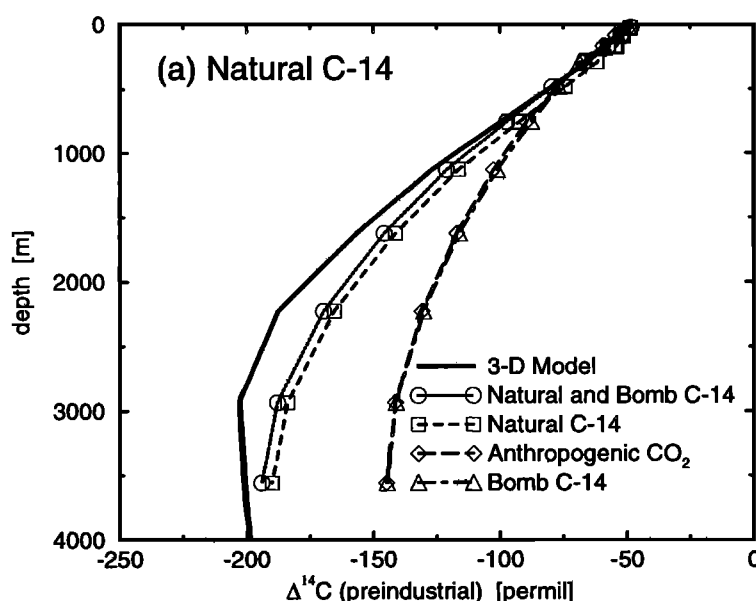

Figure 9. Tracer concentrations versus depth as simulated for the GFDL 3-D model (solid) and different versions of a B-D model. Results are shown for B-D model versions B1 natural, steady state ^{14}C(dashed, squares), B3 bomb-produced ^{14}C (1974) (dash-dotted, triangles), B5 anthropogenic CO_2 (1990) (long-dashed, diamonds), and B6 bomb ^{14}C (at the surface) and natural ^{14}C (at depth, dotted, circles).
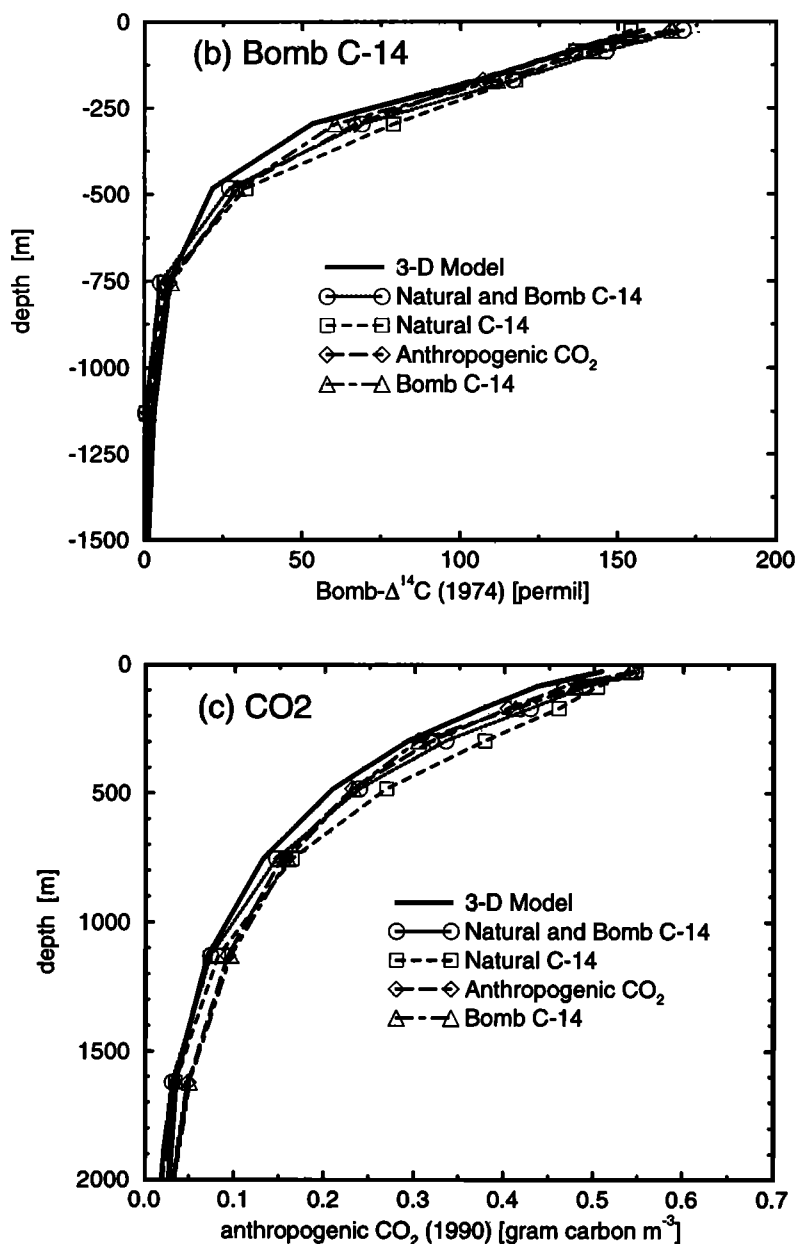
Figure 9. (continued)

large. Again, these values were extrapolated from shallower levels to the deep ocean, where it was not possible to use K_{ap} from 3-D model results. The best agreement (within 3%) with the 3-D model's CO_2 uptake and bomb-^{14}C penetration depth was found for box-model version B6 (for which K_{ap} are derived from bomb and natural ^{14}C). We conclude that the uncertainty in global oceanic CO_2 uptake estimates due to the diffusion parameterization was within 10% for our B-D model tuned with ^{14}C.

Table 1 also reveals that the uptake of anthropogenic CO_2 and the bomb-^{14}C penetration depth were not correlated for the six B-D model versions B1–B6 and the 3-D model. Thus we found that normalizing a model's anthropogenic CO_2 uptake by its simulated bomb-^{14}C

penetration depth [*Siegenthaler and Sarmiento*, 1993] requires closer inspection.

4.5. Pulse Experiments

Because the oceanic uptake of anthropogenic carbon is to the first order a linear process, its dynamics can be approximately characterized by its pulse response function. Normalized atmospheric pulse response functions are usually obtained by monitoring the decrease of an atmospheric CO_2 perturbation due to an instantaneous carbon input at time zero [*Maier-Reimer and Hasselmann*, 1987]. We have run analogous pulse experiments (pulse size and background CO_2 level are 280 ppm) for the 3-D model and B-D model versions B1, B3, B5, and B6 (Figure 10), as a means to further study the perfor-
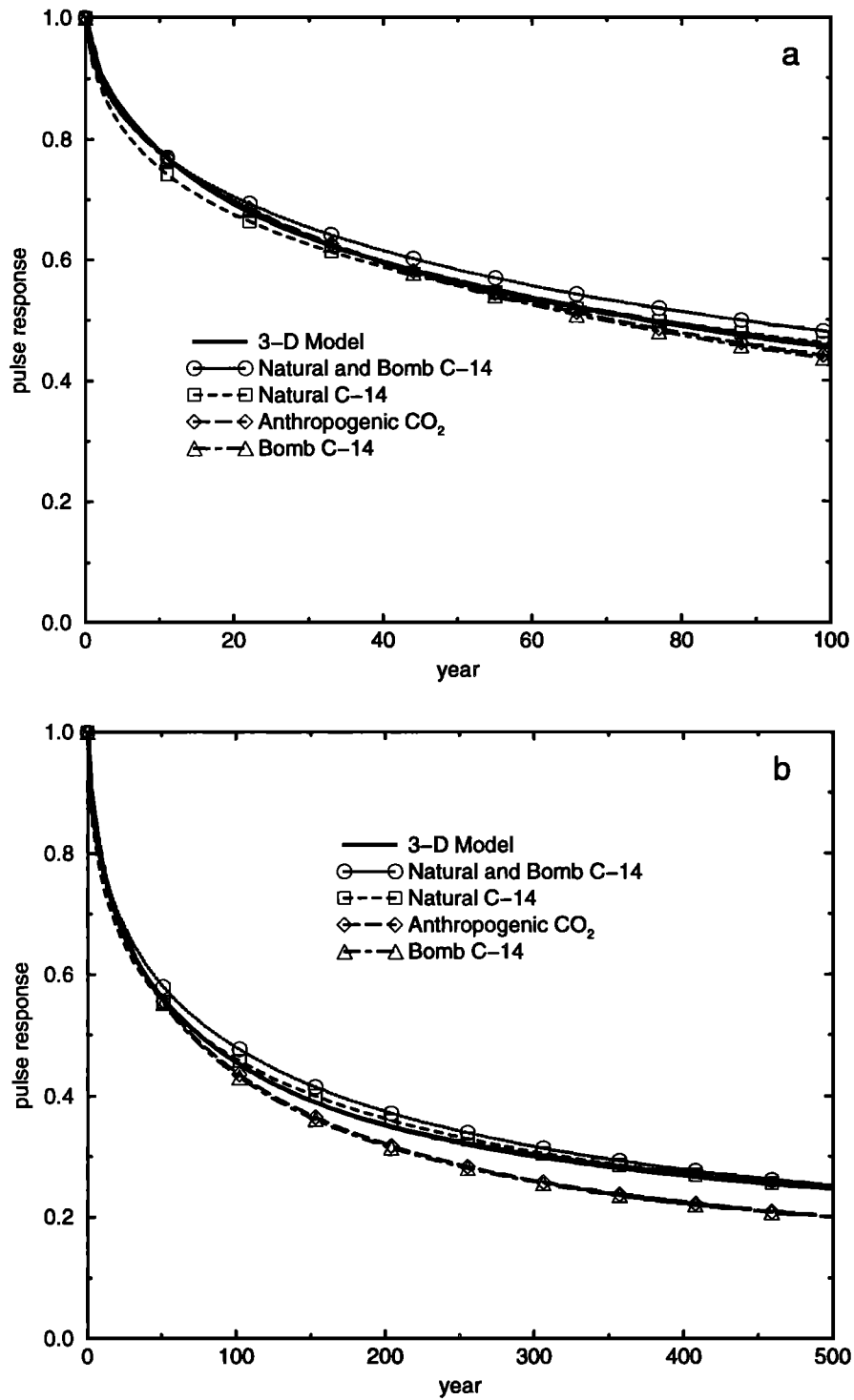
Figure 10. Response of the atmospheric CO_2 concentration to a pulse input at time $t=0$, corresponding to 100% increase of the preindustrial CO_2 concentration (280 ppm). Results are shown for the GFDL 3-D model and for the B-D model simulations that employ K_{ap} derived from 3-D results: B1 natural ^{14}C, B3 bomb-produced ^{14}C, B5 anthropogenic CO_2, and B6 bomb ^{14}C results (at the surface) and natural [14]C (at depth). The initial value of the pulse is representated here as being normalized to 1. Line signatures are as in Figure 9.

mance of the different models over different timescales.

For short timescales (<20 years), the pulse response function for the 3-D GCM agreed well with those from B-D model simulations driven by K_{ap} from 3-D runs for both anthropogenic CO_2 (B5) and bomb ^{14}C (B3). On the other hand, too much CO_2 was taken up by the B-D model simulation that employed K_{ap} from the 3-D run for natural ^{14}C (B1). The discrepancy results from K_{ap} in the surface layer being much larger for the 3-D simulation for natural ^{14}C relative to those from 3-D runs for CO_2 (Figure 6). For longer time scales (>70 years), too much CO_2 was taken up by B-D model simulations whose K_{ap} were derived from 3-D simulations for CO_2 and bomb ^{14}C. Recall, however, that K_{ap} from 3-D simulations for CO_2 and bomb ^{14}C could only be computed for the upper layers. The arbitrarily specified values for the deeper layers were clearly too large. In contrast, results from the B-D model simulation with K_{ap} from the 3-D run for natural ^{14}C agreed well with the 3-D model's long-term (>400 years) CO_2 uptake. Combining K_{ap} from bomb ^{14}C and natural ^{14}C(B6) yielded good agreement on both short and on long timescales.

4.6. Regional K_{ap}

Next, we analyzed how apparent diffusivities varied regionally. It is of interest to compare our K_{ap} with those used in another box model, the high-latitude exchange/interior diffusion-advection (HILDA) model. The HILDA model [Shaffer and Sarmiento, 1995] includes two well-mixed surface boxes, in low (50°S to 60°N) and high latitudes, a well-mixed high-latitude deep-water box, and a diffusive-interior deep-water box. Siegenthaler and Joos [1992] determined HILDA's transport parameters in order to reproduce the oceanic distributions of both natural and bomb ^{14}C, simultaneously. To match measurements, mid and low-latitude diffusivities in HILDA must decrease (from 7526 m^2 yr^{-1} at the base of the mixed layer to 465 m^2 yr^{-1} at depth). For the high latitudes, it is unfortunate that one cannot employ the southern boundary of HILDA's low- and midlatitude region for analysis of 3-D model results; in the 3-D model, this southern boundary bisects the large overturning cell in the Southern Ocean. Because K_{adv} represents transport by the ocean's large overturning cells (equation (6), section 3.2), it should be evaluated only in regions that contain such cells in their entirety.

For a qualitative comparison, we calculated K_{ap} for the region between 31°S–27°N in the 3-D model. The 3-D diffusivities decrease rapidly with depth (as they do in HILDA): from 3200 m^2 yr^{-1} to 710 m^2 yr^{-1} for K_{ap} derived from anthropogenic CO_2, from 9900 to 520 m^2 yr^{-1} for those derived from bomb ^{14}C, and from 7700 to 940 m^2 yr^{-1} for those derived from natural ^{14}C (Figure 6b). Values below about 800 m are close to the explicit diffusivity used in the 3-D model, so that advection transported little tracer to depth.

Because the equilibration time of surface water with the atmosphere is about 10 times more rapid for CO_2 than for $^{14}C/^{12}C$, CO_2 surface concentrations are relatively smoother. This resulted in a poorer correlation between the velocity field and the surface concentration for anthropogenic CO_2 as compared to bomb ^{14}C. Thus bomb ^{14}C's more pronounced minimum in the upwelling equatorial region and its maxima in the midgyre regions (Figure 2) produced larger K_{ap} than those from CO_2.

Despite this difference between individual profiles, it seems remarkable that apparent diffusivities decrease with depth. Following the argument used to explain the temporal evolution of K_{adv} derived from bomb ^{14}C, one would on the contrary expect relatively small values at the surface and large values at depth. That is, at the surface, tracer input by air-sea exchange tends to smooth concentration differences between upwelling and downwelling regions, thereby removing the correlation between velocity field and concentration field (the numerator in equation (6)). Below the surface, this correlation increased, as high concentrations are found in downwelling regions. However, advective overturning was reduced at depth (Figure 1). The large K_{ap} near the surface represent the increased importance of wind- and thermohaline-driven vertical mixing and exchange by advection. In contrast, for temperature, K_{ap} in the top 2000 m remain at around 1000 m^2 yr^{-1}, which is the explicit eddy diffusion used in the 3-D model.

Apparent diffusivities for CO_2 and ^{14}C were large for the latitudinal band 90°S–31°S (Figure 6c) because of rapid mixing. For this convective region, however, apparent diffusivities for temperature are negative. Thus heat is transported on average from cool to warm regions (i.e., the temperature flux goes against the mean temperature gradient), which violates the basic assumption behind the principal of eddy diffusion. In the Southern Ocean, the eddy diffusion approach fails for temperature because of local formation of cold and dense water. This process is responsible for the exchange of relatively warm water at depth with cool water originating from the surface. It occurs locally, regardless of the average surface-to-deep temperature gradient in the Southern Ocean.

5. Discussion

Apparent diffusivities derived from the 3-D GFDL model generally agree with those found for B-D models calibrated with ^{14}C [Siegenthaler and Oeschger, 1987; Siegenthaler and Joos, 1992]. Furthermore, they also generally agree in magnitude with those found in earlier modeling efforts [e.g., Munk, 1966].

The magnitude of the diffusivity depends on the processes parameterized and on the length scale considered. For instance, microstructure measurements of temperature, density, and velocity typically yield vertical diffusivities 10-100 times smaller [e.g., Garrett, 1979]. Corroborating these lower values is the more recent work

by *Ledwell et al.* [1993], who were able to estimate an annual-average diapycnal diffusivity of 470 m^2 yr^{-1} by releasing an inert tracer SF_6 into the thermocline and then following it with time.

The K_{ap} in the 3-D model decrease with depth in the mid and low latitudes because mixing is more vigorous near the surface. This structure agrees with that found by calibrating the HILDA model with ^{14}C [*Siegenthaler and Joos*, 1992]. However, these model results seem to contradict both theoretical considerations that describe mixing as being inversely related to water column stability [e.g., *Welander*, 1968] and measurements of of ^{222}Rn and ^{228}Ra near the ocean bottom [*Sarmiento et al.*, 1976]. From the latter study's relationship between diffusivity and the buoyancy gradient, diffusivities should increase with depth, from lows of roughly 100 m^2 yr^{-1} at 100 m to highs of order 10,000 m^2 yr^{-1} in the deep ocean.

What could explain these large discrepancies? It seems but a question of scale. Diffusivities in box models represent transport not only by local mixing, but also that due to advection (from large-scale overturning cells) and convection. Furthermore, box models consider vertical transport along isopycnals (which is thousands of times more important than is diapycnal mixing [*Ledwell et al.*, 1993]) to be a component of the vertical eddy diffusivity. The decrease of box-model eddy diffusivities with depth reflects in part the flattening out of isopycnals as one moves away from the surface.

Regarding box-model validation, we found that apparent diffusion coefficients derived from bomb and natural ^{14}C gave reliable results (to within 10%) for B-D model estimates of the global CO_2 uptake. Furthermore, the agreement between the different versions of the B-D model has confirmed earlier work by *Siegenthaler and Joos* [1992] showing that simultaneous use of bomb and natural ^{14}C offers a good means, currently the best, to calibrate box models designed to estimate global ocean uptake of anthropogenic CO_2. The same utility does not hold for other tracers which have substantially different temporal histories, sources, and sinks. We have shown temperature not to be a suitable tracer to determine transport coefficients for parameterized carbon-cycle models because the processes governing the global temperature distribution are markedly different from those governing the downward transport of carbon and ^{14}C. Similarly, any tracer strongly related to the temperature distribution cannot a priori be properly represented by B-D models tuned with ^{14}C. However, one must distinguish between the ocean's steady state temperature distribution and the penetration of a temperature perturbation into the ocean, that is, as results from climate change. *Bryan et al.* [1983] found that the penetration of a small positive temperature anomaly (+0.5°C) in the GFDL 3-D model is analogous to the penetration of a passive tracer like anthropogenic CO_2.

Apparent diffusivities derived for bomb ^{14}C varied with time. Yet approximating them as constant, that is, by calibrating box models with observations of bomb ^{14}C, appeared to present no serious problem. Still, though, when simulating bomb ^{14}C uptake with a box model, one approaches the limits of the eddy diffusion parameterization because timescales governing the bomb-^{14}C history are short.

As concerns 3-D modeling efforts, this study suggests that tracers exhibiting rapid increases in the atmosphere and a fast air-sea equilibration (e.g., the chlorofluorocarbons (CFCs) or SF_6) are better than ^{14}C to test the convective scheme of 3-D models. This conclusion is supported by the large contribution by convection, in the GFDL model, to the global downward transport of anthropogenic CO_2 (40%) and of bomb ^{14}C until 1964. On the other hand, the importance of convection for the downward transport of bomb ^{14}C decreased rapidly in the GFDL model after the peak in atmospheric ^{14}C, and it was always small for the downward transport of natural ^{14}C. However, convection still has an impact on modeled radiocarbon concentrations.

The close agreement between these B-D and 3-D model simulations for both anthropogenic CO_2 and bomb ^{14}C suggests that B-D models and their inherent eddy diffusion approach are appropriate to study the global oceanic uptake of anthropogenic CO_2. Disagreement (10%) between the different versions of the B-D model is of equal order to uncertainties associated with present-day estimates for ocean inventories of bomb ^{14}C and anthropogenic CO_2 [*Schimel et al.*, 1995]. Nonlinearities associated with locally different gas exchange rates, carbon chemistry, and ocean circulation (all included in the 3-D model but not in the B-D model) appear to make little difference in the global uptake.

Appendix: Calculation of Apparent Diffusivities

In the GFDL 3-D model, grid boxes defining the model's geometry are labeled with three indices i, j, k, thereby determining position in x,y,z space [*Bryan*, 1969]. With the index $k - 1/2$ to label quantities defined at the top side of each grid box, one can write the flux per unit area leaving grid box (i, j, k) in the upward direction as

$$f_{i,j,k-1/2} = w_{i,j,k-1/2} c_{i,j,k-1/2}$$
$$-A_{v;k-1/2} \frac{c_{i,j,k-1} - c_{i,j,k}}{\Delta z_{k-1/2}} + \text{convection}$$
$$= f_{adv} + f_{diff} + f_{conv}, \qquad (A1)$$

and the corresponding total mass flux as

$$F_{i,j,k-1/2} = a_{i,j,k-1/2} f_{i,j,k-1/2}, \qquad (A2)$$

where f_{adv}, f_{diff}, and f_{conv} denote the advective, diffusive, and convective component of the total tracer flux (indices omitted for simplicity), $a_{i,j,k-1/2}$ is the area of the top side, and $w_{i,j,k-1/2}$ is the upward velocity averaged over this top side (as computed in the 3-D GCM by solving its primitive equations). As for tracer concentration, $c_{i,j,k}$ represents the volume average for grid box (i, j, k) and $c_{i,j,k-1/2}$ that which is advected (i.e., the mean of $c_{i,j,k}$ and $c_{i,j,k-1}$). In the diffusion term, the fraction is the gradient of the averaged tracer concentration in vertical direction, as represented by the model's centered differencing scheme. The symbol $\Delta z_{k-1/2}$ signifies the distance between the midpoints of layers k and $k-1$. The 3-D model's diffusion matrix is diagonal with respect to the model coordinate system, and for each vertical level, explicit diffusion coefficients (denoted by Bryan and coworkers as A_v) are taken as constants.

In the nonseasonal 3-D model of *Toggweiler et al.* [1989a], after a 2009-year integration, temporal fluctuations of the transport field are small; in the off-line version [*Najjar*, 1990; *Sarmiento et al.*, 1992], there are no fluctuations, by definition. Therefore we neglected the contribution of transient eddies to the extent that they are not taken into account by the 3-D model's explicit diffusion, and we calculated K_{ap} at discrete times for which 3-D model results are available. Concentration, flux, and velocity fields were horizontally averaged, and the vertical K_{ap} at depth $z_{k-1/2}$ was calculated as

$$K_{ap}(z_{k-1/2}) = \frac{\langle w_{i,j,k-1/2}\rangle\langle c_{i,j,k-1/2}\rangle}{\frac{\langle c_{i,j,k-1}\rangle - \langle c_{i,j,k}\rangle}{\Delta z_{k-1/2}}}$$
$$- \frac{\langle f_{i,j,k-1/2}\rangle}{\frac{\langle c_{i,j,k-1}\rangle - \langle c_{i,j,k}\rangle}{\Delta z_{k-1/2}}} , \qquad (A3)$$

which can be split into the sum of three components defined by the 3-D model's advective, diffusive, and convective tracer fluxes:

$$K_{adv}(z_{k-1/2}) = \frac{\langle w_{i,j,k-1/2}\rangle \cdot \langle c_{i,j,k-1/2}\rangle}{\frac{\langle c_{i,j,k-1}\rangle - \langle c_{i,j,k}\rangle}{\Delta z_{k-1/2}}}$$
$$- \frac{\langle f_{adv}\rangle}{\frac{\langle c_{i,j,k-1}\rangle - \langle c_{i,j,k}\rangle}{\Delta z_{k-1/2}}} \qquad (A4)$$

$$K_{diff}(z_{k-1/2}) = \frac{-\langle f_{diff}\rangle}{\frac{\langle c_{i,j,k-1}\rangle - \langle c_{i,j,k}\rangle}{\Delta z_{k-1/2}}} \qquad (A5)$$

$$K_{conv}(z_{k-1/2}) = \frac{-\langle f_{conv}\rangle}{\frac{\langle c_{i,j,k-1}\rangle - \langle c_{i,j,k}\rangle}{\Delta z_{k-1/2}}} \qquad (A6)$$

Again, angle brackets define the horizontal average. K_{diff} equals the 3-D model's explicit diffusivity A_v, to within the numerical limits of the averaging procedure. For the global ocean, the mean vertical water velocity $\langle w_{i,j,k-1/2}\rangle$ is zero.

References

Berger, W.H., K. Fischer, C. Lai, and G. Wu, Ocean productivity and organic carbon flux, I, Overview and maps of primary production and export production, *SIO Ref. 87-30*, Scripps Inst. of Oceanogr., La Jolla, Calif., 1987.

Bolin, B. (Ed.), *Carbon Cycle Modelling*, 390 pp., John Wiley, New York, 1981.

Broecker, W. S., and T.-H. Peng, The role of CaCO3 compensation in the glacial to interglacial atmospheric CO2 change, *Global Biogeochem. Cycles, 1*, 15-39, 1987.

Broecker, W. S., T.-H. Peng, G. Östlund, and M. Stuiver, The distribution of bomb radiocarbon in the ocean, *J. Geophys. Res., 90*, 6953-6970, 1985.

Broecker, W. S., S. Sutherland, W. Smethie, T.-H. Peng, and G. Östlund, Oceanic radiocarbon: Separation of the natural and bomb components, *Global Biogeochem. Cycles, 9*, 263-288, 1995.

Bryan, K., A numerical method for the study of the circulation of the world ocean, *J. Comput. Phys., 4*, 347-376, 1969.

Bryan, K., Models of the world ocean, *Dyn. Atmos. Oceans, 3*, 327-338, 1979.

Bryan, K., and L. J. Lewis, A water mass model of the world ocean circulation, *J. Geophys. Res., 84*, 2503-2517, 1979.

Bryan K., F. G. Komro, and C. Rooth, The ocean's transient response to global surface temperature anomalies, in *Climate Processes and Climate Sensitivity, Geophys. Monogr. Ser.*, vol. 29, edited by J. E. Hansen and T. Takahashi, pp. 29-36, AGU, Washington, D. C., 1984.

Ciais, P., P. P. Tans, M. Trolier, J. W. C. White, and R. J. Francey, A large Northern Hemispheric terrestrial CO2 sink indicated by the ^{13}C/^{12}C ratio of atmospheric CO2, *Science, 269*, 1098-1102, 1995.

Enting, I. G., T. M. L. Wigley, and M. Heimann, Future emissions and concentrations of carbon dioxide: Key ocean/atmosphere/land analyses, *Tech. Pap. 31*, pp.

120, Div. of Atmos. Res., Commonw. Sci. and Ind. Res. Org., Melbourne, Victoria, 1994.

Eppley, R. W., and B. J. Peterson, Particulate organic matter flux and planktonic new production in the deep ocean, Nature, 282, 677-680, 1979.

Esbensen, S. K., and Y. Kushnir, The heat budget of the global ocean: An atlas based on estimates from surface marine observations, Rep. 29, Clim. Res. Inst., Oreg. State Univ., Corvallis., 1981.

Fiadeiro, M.E., Three-dimensional modeling of tracers in the deep Pacific Ocean, II, Radiocarbon and the circulation, J. Mar. Res., 40, 537-550, 1982.

Friedli, H., H. Loetscher, H. Oeschger, U. Siegenthaler, and B. Stauffer, Ice core record of the $^{13}C/^{12}C$ ratio of atmospheric carbon dioxide in the past two centuries, Nature, 324, 237-238, 1986.

Garrett, C., Mixing in the ocean interior, Dyn. Atmos. Oceans, 3, Elsevier, Amsterdam, 239-265, 1979.

Gaspar, P., Y. Gregorius, and J.-M. Lefevre, A simple eddy kinetic energy model for simulations of oceanic vertical mixing: Tests at Station Papa and Long-Term Upper Ocean Study Site, J. Geophys. Res., 95, 16179-16193, 1990.

Harvey, L. D. D., Effect of the ocean mixing on the transient climate response to a CO_2 increase: Analysis of recent model results, J. Geophys. Res., 91, 2709-2718, 1986.

Hesshaimer, V., M. Heimann, and I. Levin, Radiocarbon evidence for a smaller oceanic carbon dioxide sink than previously believed, Nature, 370, 201-203, 1994.

Joos, F., Bomb radiocarbon: Imbalance in the budget, Nature, 370, 181-182, 1994.

Joos, F., J. L. Sarmiento, and U. Siegenthaler, Estimates of the effect of Southern Ocean iron fertilization on atmospheric CO_2 concentrations, Nature, 349, 772-775, 1991.

Keeling, C. D., R. B. Bacastow, A. F. Carter, S. C. Piper, T. P. Whorf, , M. Heimann, W. G. Mook, and H. Roeloffzen, A three-dimensional model of atmospheric CO_2 transport based on observed winds, 1. Analysis of observational data, in Aspects of Climate Variability in the Pacific and Western Americas, Geophys. Monogr. Ser., vol. 55, Washington D. C., edited by D. H. Peterson, pp 165-236, AGU, 1989.

Keeling, R. F., and S. R. Shertz, Seasonal and interannual variations in atmospheric oxygen and implications for the global carbon cycle, Nature, 358, 723-727, 1992.

Kurz, K. D., and E. Maier-Reimer, Iron fertilization of the Austral Ocean—The Hamburg model assessment, Global Biogeochem. Cycles, 7, 229-244, 1993.

Ledwell, J. R., A. J. Watson, and C. S. Law, Evidence of slow mixing across the pycnocline from an open-ocean tracer-release experiment, Nature, 364, 701-703, 1993.

Mahlman, J. D., Some fundamental limitations of simplified-transport models as implied by results from a three-dimensional general-circulation/tracer model. in Proceedings of the Fourth Conference on the Climatic Impact Assessment Program, edited by T. M. Hard and A. J. Broderick, pp. 132-146, U.S. Dep. of Transp., Washington D. C., 1975.

Maier-Reimer, E., and K. Hasselmann, Transport and storage of CO_2 in the ocean—an inorganic ocean-circulation carbon cycle model, Clim. Dyn., 2, 63-90, 1987.

Munk, W. H., Abyssal recipes, Deep-Sea Res., 13, 707-730, 1966.

Najjar, R. G., Simulations of the phosphorus and oxygen cycles in the world ocean using a general circulation model, Ph.D. thesis, 190 pp., Princeton Univ., Princeton, N. J., 1990.

Najjar, R. G., Downward transport and fate of organic mat-

ter in the ocean: simulations with a general circulation model, Global Biogeochem. Cycles, 6, 45-76, 1992.

Neftel, A., E. Moor, H. Oeschger, and B. Stauffer, Evidence from polar ice cores for the increase in atmospheric CO_2 in the past two centuries, Nature, 315, 45-47, 1985.

Newell, R. E., The general circulation of the atmosphere and its effects on the movement of tracer substances, J. Geophys. Res., 68, 3949-3962, 1963.

Oeschger, H., U. Siegenthaler, U. Schotterer, and A. Gugelmann, A box diffusion model to study the carbon dioxide exchange in nature, Tellus, 27, 168-192, 1975.

Packard, T. T., M. Denis, M. Rodier, and P. Garfield, Deep-ocean metabolic CO_2 production: Calculations from ETS activity, Deep-Sea Res., Part A, 35, 371-382, 1988.

Peixoto, J. P., and A.H. Oort, Physics of Climate, Am. Inst. of Phys., New York, pp. 61-65, 1992.

Plumb, R. A., and Mahlman, J.D., The zonally averaged transport characteristics of the GFDL general circulation/transport model. J. Atmos. Science 44, 298-327, 1987.

Redi, M. H., Oceanic isopycnal mixing by coordinate rotation, J. Phys. Oceanogr., 12, 1154-1158, 1982.

Revelle, R., and H. E. Suess, Carbon dioxide exchange between atmosphere and ocean and the question of an increase of atmospheric CO_2 during past decades, Tellus, 9, 18-27, 1957.

Sarmiento, J. L., A simulation of bomb tritium entry into the North Atlantic Ocean, J. Phys. Oceanogr., 13, 1924-1939, 1983.

Sarmiento, J.L., W. H. Feely, W. S. Moore, A. E. Bainbridge, and W. S. Broecker, The relationship between vertical eddy diffusion and buoyancy gradient in the deep sea, Earth Planet. Sci. Lett., 32, 357-370, 1976.

Sarmiento, J. L., J. C. Orr, and U. Siegenthaler, A perturbation simulation of CO_2 uptake in an ocean general circulation model, J. Geophys. Res., 97, 3621-3645, 1992.

Schimel, D., I. G. Enting, M. Heimann, T. M. L. Wigley, D. Raynaud, D. Alves, and U. Siegenthaler, CO_2 and the carbon cycle, in Climate Change 1994, edited by J. T. Houghton, L. G. Meira Filho, J. Bruce, H. Lee, B. A. Callander, E. Haites, N. Harris, and K. Maskell, pp. 35-71, Int. Panel on Clim. Change, Cambridge Univ. Press, New York, 1995.

Schlesinger, M. E., and X. Jiang, Simple model representation of atmosphere-ocean GCMs and estimation of the time scale of CO_2-induced climate change, J. Climate, 3, 1297-1315, 1990.

Shaffer, G., and J. L. Sarmiento, Biogeochemical cycling in the global ocean, 1, A new, analytical model with continuous vertical resolution and high-latitude dynamics, J. Geophys. Res., 100, 2659-2672, 1995.

Siegenthaler U., and F. Joos, Use of a simple model for studying oceanic tracer distributions and the global carbon cycle, Tellus, Ser. B, 44, 186-207, 1992.

Siegenthaler, U., and H. Oeschger, Transient temperature changes due to increasing CO_2 using simple models, Ann. Glaciol. 5, 153-159, 1984.

Siegenthaler, U., and H. Oeschger, Biospheric CO_2 emissions during the past 200 years reconstructed by deconvolution of ice core data, Tellus, Ser. B, 39, 140-154, 1987.

Siegenthaler, U., and J. L. Sarmiento, Atmospheric carbon dioxide and the ocean, Nature, 365, 119-125, 1993.

Siegenthaler, U., and T. Wenk, Rapid atmospheric CO_2 variations and ocean circulation, Nature, 308, 624-625, 1984.

Toggweiler, J. R., K. Dixon, and K. Bryan, Simulations of radiocarbon in a coarse resolution world ocean model, 1, Steady state prebomb distributions, J. Geophys. Res., 94, 8217-8242, 1989a.

Toggweiler, J. R., K. Dixon, and K. Bryan, Simulations of radiocarbon in a coarse.resolution world ocean model, 2, Distributions of bomb-produced carbon 14, *J. Geophys. Res.*, *94*, 8243–8264, 1989b.

Welander, P., Theoretical forms for the vertical exchange coefficients in a stratified fluid with applications to lakes and seas, *Acta R. Soc. Sci. Litt. Gothob. Geophys.*, vol. I, Gothenburg, Sweden, 1968.

Walsh, J., A data set on northern hemisphere sea ice extent, 1953-76, Glacialogical data, *Report SD-2*, pp 49–51 World Data Cent. A for Glaciol. [Snow and Ice], Boulder, Colo., 1978.

Yin, F.L., and I. Y. Fung, Net diffusivity in ocean general circulation models with nonuniform grids. *J. Geophys. Res.*, *96*, 10773-10776, 1991.

Zwally, H.J., J. Comiso, C. Parkinson, W. Campbell, F. Carsey, and P. Gloerson, Antarctic sea ice, 1973-76: Satellite passive microwave observations, *NASA Publ.*, 206 pp., 1983.

F. Joos,   Physics Institute, University of Bern, Sidlerstr. 5, CH-3012 Bern, Switzerland. (e-mail:joos@climate.unibe.ch)

J. C. Orr, CEA/DSM, Laboratoire de Modélisation du Climat et de l'Environnement, Orme des Merisiers, Bât. 709, F-91191 Gif-sur-Yvette, France. (e-mail:orr@cea.fr)